Supplementary Information (SI) for Dalton Transactions.

Supporting Information

A zirconocene triazenido hydride complex activates CO_2

Charlotte Proges[a], Kevin Lindenau[a], Julia Rothe[a,b], Anke Spannenberg[a], Wolfgang Baumann,[a] Fabian Reiß*[a], Axel Schulz[a,b] and Torsten Beweries*[a]

[a] *Leibniz Institute for Catalysis, Albert-Einstein-Str. 29a, 18059 Rostock, Germany. Email:* *fabian.reiss@catalysis.de*, *torsten.beweries@catalysis.de*

[b] *University of Rostock, Institute of Chemistry, 18059 Rostock, Germany.*

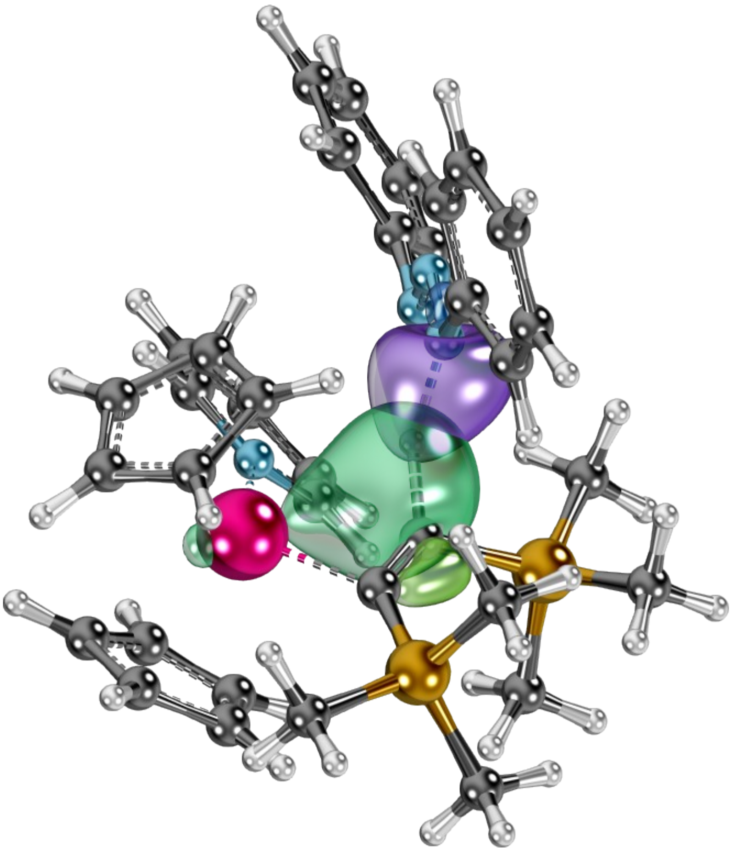

Table of contents

1 Experimental details

1.1 General

All manipulations were carried out in an oxygen- and moisture-free argon atmosphere using standard Schlenk and drybox techniques. The solvents were purified with the Grubbs-type column system “Pure Solv MD-5” and dispensed into thick-walled glass Schlenk bombs equipped with Young-type Teflon valve stopcocks. The following compounds were prepared according to literature procedures: $Cp_2Zr(py)Me_3SiCCSiMe_3$ [1], 1,3-diphenyltriazene (PhNNN(H)Ph)[2]. The liquid compounds bis(trimethylsilyl)acetylene ($Me_3SiCCSiMe_3$, TCI, > 97%), Diethylsilane (Et_2SiH_2, Sigma-Aldrich, >97%), 1,8-Diazabicyclo(5.4.0)undec-7-ene (DBU, TCI, >98%), triethylamine (NEt_3, TCI, >99%) and pyridine (TCI, > 99%) were dried using molecular sieves (3Å), then distilled and stored in a refrigerator before use. Commercially available *n*-BuLi solution (1.6 M and 2.5 M in *n*-hexane, Acros) and bis(cyclopentadienyl)zirconium(IV) dichloride (Cp_2ZrCl_2, >98%, Aldrich), were transferred into Schlenk tubes, stored under argon and used as received.

NMR spectra were recorded on Bruker AV300 and AV400 spectrometers. ^1H and ^{13}C chemical shifts were referenced to the solvent signal: benzene-d_6 (δ_H = 7.16 ppm, δ_C = 128.06 ppm), THF-d_8 (δ_H = 1.73 ppm, δ_C = 25.2 ppm).[3] Chemical shifts of ^{15}N were determined by indirect detection and are given relative to a reference frequency calculated from the actual ^1H reference frequency and $\Xi(^{15}N)$ = 10.136 767 MHz[4] (which corresponds to neat nitromethane at 0 ppm). Each determination was carried out at least twice with variation of carrier frequency and spectral range in the indirect dimension to ensure that the signals are not folded along the F_1 axis. Reaction monitoring was performed on a Spinsolve benchtop 80 MHz spectrometer (Magritek).

IR spectra were recorded on a Bruker Alpha FT-IR, ATR Spectrometer, spectra are not corrected.

MS analysis was done using a Finnigan MAT 95-XP instrument (Thermo-Electron) in CI^+/CI^- mode (isobutene) and for the air stable compounds in EI mode.

CHN analysis was using a Leco TruSpec elemental analyser. At this point it should be pointed out that we could not obtain satisfactory elemental analysis. Despite repeated recrystallisation, repeated measurements with and without oxidizer V_2O_5 and modified furnace temperature, we observed up to 10% less carbon content than calculated/expected. This behaviour might be explained by formation of mixed zirconium-carbides (ceramics) in the furnace and therefore the carbon content dramatically decreases.[5]

X-Ray diffraction data were collected on a Bruker Kappa APEX II Duo diffractometer. The structures were solved by direct methods (SHELXS-97)[6] and refined by full-matrix least-squares procedures on F^2 (SHELXL-2014 and SHELXL-2018, respectively).[7] Diamond was used for graphical representations.[8]

DFT calculations were carried out with the Gaussian 16 package of molecular orbital programs Preoptimisation of reaction paths was performed with help of Grimme’s semiempirical tool GFN-xTB2. For further details see section 6.

1.2 Synthesis of $Cp_2Zr(py)(\eta^2\text{-}Me_3SiCCSiMe_3)$ (complex 1)

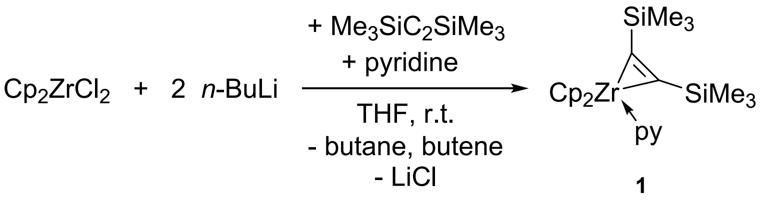

Complex **1** was prepared according to literature procedure. A Schlenk tube was charged with 4.996 g (17.1 mmol, 1.0 eq.) Cp_2ZrCl_2 in the glove box, to this tube 2.910 g bis(trimethylsilyl)acetylene (17.1 mmol, 1.0 eq.) and 100 mL THF were added. The solution was cooled to -78 °C and 13.7 mL (2.5 M, 34.3 mmol, 2.0 eq.) of *n*-BuLi was added dropwise over a period of 15 min, while stirring. After this the solution turned clear yellow. The solution was allowed to warm to room temperature within two hours, resulting in a colour change to a dark brown red. Pyridine (1.4 mL, 17.4 mmol, 1.0 eq.) was added and the colour changed to dark purple. The volume of the solution was reduced to 20-30 mL and 200 mL of pentane was added and the mixture was stirred for 30 min. The solution was transferred into a new Schlenk flask via canula filtration and stored at -60 °C overnight. The remaining solution was removed using a canula filter and the precipitated solid was washed twice with cold (-78 °C) pentane. The product was obtained as a crystalline dark purple solid (3.608 g, 7.66 mmol, 43%).

^{1}**H NMR** (400 MHz, benzene-d_6): δ = 0.32 (br s, 18H, $Si(CH_3)_3$) 5.47 (s, 10 H, Cp), 6.41 (m, 2H, pyridine), 6.80 (m, 1H, pyridine), 8.84 ppm (m, 2H, pyridine).

1.3 Monitoring of the reaction of complex 1 and 1,3-diphenyltriazene

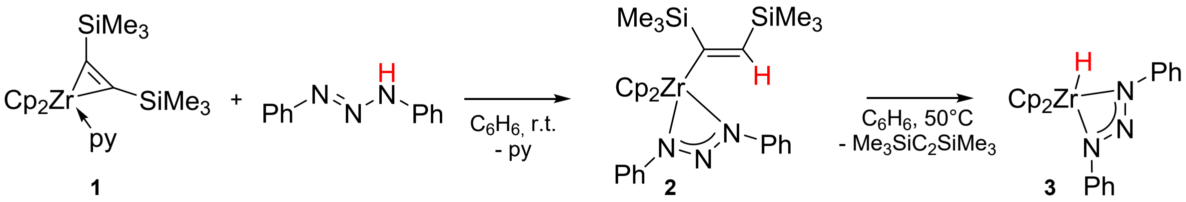

In a glove box, 20.8 mg (0.105 mmol, 4.8 eq.) of 1,3-diphenyltriazene and 10.4 mg (0.022 mmol, 1 eq.) of **1** were placed in an NMR tube, 0.7 mL of benzene-d_6 was added and the solution was immediately frozen (-78 °C). Before the first measurement, the mixture was warmed to room temperature and shaken. ^{1}H NMR spectra were then recorded every 30 minutes for a period of 75 hours (for selected spectra see **Figure S1**). The relative integral ratio of the two Me_3Si groups of complex **2**, as well as for the uncoordinated $Me_3SiC_2SiMe_3$, was followed over this time. The monitoring experiment shows a rather slow reaction within this time under ambient conditions. Therefore, complex **3** was deliberately synthesised at elevated temperatures (see **Figure S2**). Of note, due to the fast exchange of pyridine by 1,3-diphenyltriazene we were not able to monitor the first reaction step shown in the scheme above.

The reported ^{1}H, ^{13}C, and ^{29}Si NMR shifts shown are from independent NMR experiments. Characteristic resonances consistent with the shown structural motif of complex **2** have been identified from 2D NMR spectra (see section 2.2).

^{1}H NMR (400 MHz, 25°C, benzene-*d*$_6$): δ = 7.42 (m, approx. 4H, Ph), 6.81 (s, 1H, ((H$_3$C)$_3$SiC(*H*)CSi(CH$_3$)$_3$),), 5.70 (s, 10H, Cp), 0.36 (s, 9H, Si(C*H*$_3$)$_3$), -0.03 ppm (s, 9H, CHSi(C*H*$_3$)$_3$). **^{13}C NMR** (101 MHz, 25°C, benzene-*d*$_6$): δ = 205.4 ((H$_3$C)$_3$SiC(H)*C*Si(CH$_3$)$_3$), 143.0 ((H$_3$C)$_3$Si*C*(H)CSi(CH$_3$)$_3$), 124.2 (CH, Ph), 120.4 (CH, Ph), 116.9 (CH, Ph), 110.0 (CH, Cp), 2.9 (Si(*C*H$_3$)$_3$), -0.1 ppm (CHSi(*C*H$_3$)$_3$). **^{1}H NMR** (400 MHz, -20°C, toluene-*d*$_8$): δ = 6.75 (s, 1H, (H$_3$C)$_3$SiC(*H*)CSi(CH$_3$)$_3$), 5.63 (s, 10H, Cp), 0.34 (s, 9H, Si(C*H*$_3$)$_3$), -0.05 ppm (s, 9H, CHSi(C*H*$_3$)$_3$). **^{13}C NMR** (101 MHz, -20°C, toluene-*d*$_8$): δ = 205.8 ((H$_3$C)$_3$SiC(H)*C*Si(CH$_3$)$_3$), 145.7 ((H$_3$C)$_3$Si*C*(H)CSi(CH$_3$)$_3$), 109.8 (CH, Cp), 2.9 (Si(*C*H$_3$)$_3$), 0.3 ppm (CHSi(*C*H$_3$)$_3$). **^{29}Si-inept NMR** (79 MHz, -20°C, toluene-*d*$_8$): δ = -9.7 (C*Si*Me$_3$), -11.7 ppm (CSiMe$_3$).

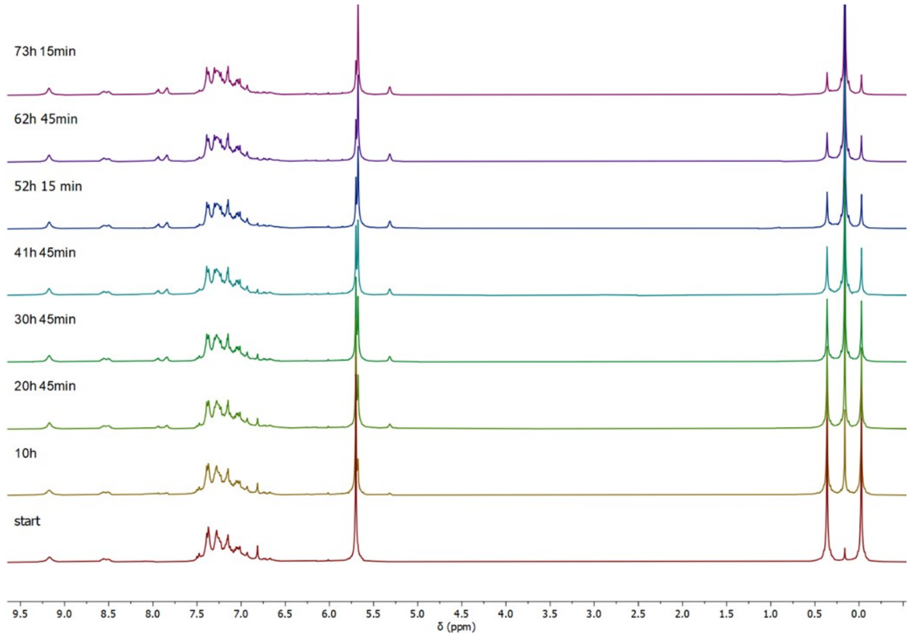

Figure S1. Selected ^{1}H NMR spectra of the monitoring of the reaction of complex **1** with 1,3-diphenyltriazene (25 °C, 80 MHz, benzene-*d*$_6$)

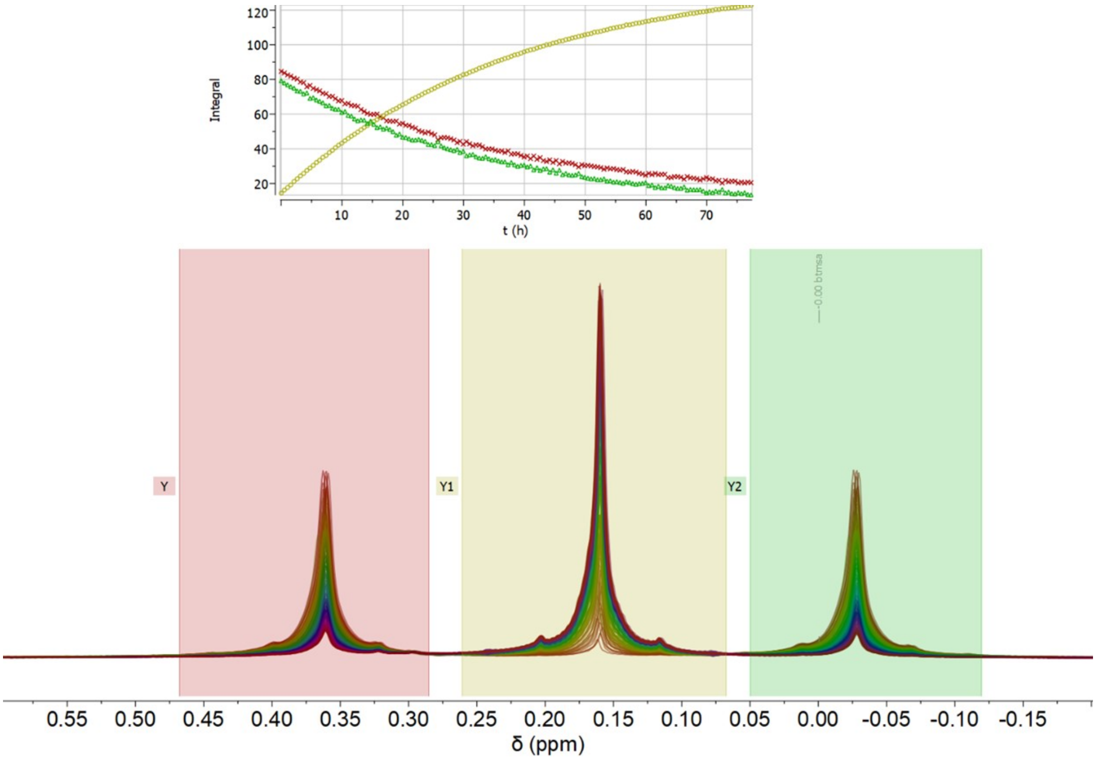

Figure S2. Top: plot of the integral of the NMR peaks in the high field region (see bottom part) over time. Bottom: Overlay of all NMR spectra recorded during reaction monitoring (only high field region shown). Signal assignment: free $Me_3SiCCSiMe_3$, 0.16 ppm; coordinated $Me_3SiCCSiMe_3$ (complex **2**), 0.36 ppm and -0.03 ppm.

1.4 Synthesis of complex 3

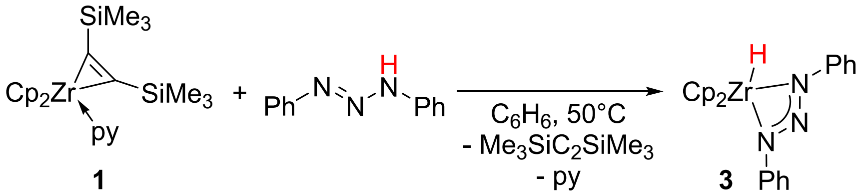

Complex **1** (601 mg, 1.28 mmol, 1 eq) and 1,3-diphenyltriazene (253 mg, 1.28 mmol, 1 eq) were placed in a Schlenk flask inside the glove box, 60 mL of benzene was added, the mixture was stirred and heated to 50 °C for 18 h, resulting in a colour change to dark red. After cooling the solution to room temperature, the volume was reduced to approximately 5 mL and 50 mL of pentane was added. This resulted in precipitation of a small amount of fluffy solid. The solution was filtered off using a cannula filter and left at -78 °C for two days, producing orange crystals, which were used for SC-XRD analysis of **3**. The solution was filtered and the crystalline solid was washed with cold (-78 °C) pentane. The remaining solvent was removed, applying vacuum for several hours. The product was obtained as an orange solid (414 mg, 0.99 mmol, 78%). Analytically pure complex **3** was obtained by repeated washing of the solid at -78 °C with cold pentane and drying in vacuum.

^{1}H NMR (300 MHz, THF-d_8): δ = 5.17 (s, 1H, Zr*H*), 6.05 (s, 10 H, Cp) 6.96 (m, 1H, *p*-CH, 1-Ph), 7.06 (m, 1H, *p*-CH, 3-Ph), 7.19 (m, 2H, *m*-CH, 1-Ph), 7.34 (m, 2H, *m*-CH, 3-Ph), 7.38 (m, 2H, *o*-CH, 3-Ph), 7.52 ppm (m, 2H, o-CH, 1-Ph). [1-Ph points to ZrH side of complex]. **^{13}C NMR** (101 MHz, THF-d_8) δ = 150.1 (*i*-C; 1-Ph), 150.0 (*i*-C, 3-Ph), 129.6 (*m*-CH, 3-Ph), 128.8 (*m*-CH, 1-Ph), 124.2 (*p*-CH,1+3-Ph), 118.6 (*o*-CH, 1-Ph), 117.3 (*o*-CH, 3-Ph), 105.7 ppm (CH, Cp). **^{1}H-^{15}N HMBC** (41 MHz, THF-d_8) δ = –122.5 (α-N, N3), –109.6 (α-N, N1), 126.6 ppm (β-N, N2). Assignment according to the SC-XRD labelling. **IR**: 3065 (w), 3032 (w), 1591 (m) 1480 (m), 1297 (m), 1271 (s), 1237 (m), 802 (m), 758 (m), 690 (m), 658 cm^{-1} (m). **Elemental analysis** calcd (%) for $C_{22}H_{21}N_3Zr$ (M = 418.66 g mol^{-1}): C, 63.12; H, 5.06; N, 10.04. Found: C, 53.76; H, 3.716; N, 9.18. **MS** (*m*/*z*, CI, *isobutene*): 474 [M + isobutene], 416 [M – H^{-}], 312 [M – N_2Ph], 105 [N_2Ph].

1.5 Synthesis of complex 4

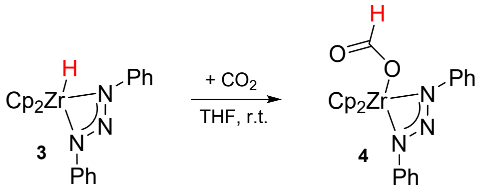

Complex **3** (175 mg, 0.42 mmol, 1 eq) was placed in a Schlenk flask and 4 mL of THF was added. The flask was then connected to a CO_2 line via the valve and fitted with a septum (using the CO_2 to maintain an inert atmosphere). A cannula was inserted and held close to the surface of the solution, exposing it to a stream of CO_2, and the solution was kept in this state and stirred for 5 minutes, during which time its colour became noticeably lighter. The solvent was then removed in vacuum. The product was obtained as a yellow-orange solid (153 mg, 0.33 mmol, 79%). Analytically pure complex **4** was obtained by repeated washing of the solid at -78 °C with cold pentane and drying in vacuum.

Crystals suitable for SC-XRD analysis were obtained when trying to grow crystals of **3** from a clear saturated THF solution after slow cooling in a Dewar vessel cooled with dry ice.

^{1}H NMR (300 MHz, THF-d_8): δ = 6.38 (s, 10H, Cp), 7.07 (m, 1H, *p*-CH, 3-Ph), 7.15 (m, 1H, *p*-CH, 1-Ph), 7.27 (m, 2H, *m*-CH, 3-Ph), 7.41 (m, 2H, *m*-CH, 1-Ph) 7.46 (m, 2H, *o*-CH, 1-Ph), 7.50 (m, 2H, *o*-CH, 3-Ph), 8.28 ppm (s, 1H, O-C*HO*, ${}^{1}J_{C,H}$ = 205 Hz, *formate*). 3-Ph points to ZrOCHO side of complex,. **^{13}C NMR** (101 MHz, THF-d_8): δ = 166.2 *(formate, ${}^{1}J_{C,H}$* =205 Hz), 150.3 (*i*-C, 1-Ph), 149.5 (*i*-C, 3-Ph), 129.8 (*m*-CH, 3-Ph), 128.8 (*m*-CH, 1-Ph), 125.0 (*p*-CH, 3-Ph), 125.0 (*p*-CH, 1-Ph), 121.2 (*o*-CH, 1-Ph), 118.4 (*o*-CH, 3-Ph), 113.6 ppm (Cp). **^{1}H-^{15}N HMBC** (41 MHz, THF-d_8): δ = –113.3 (α-N, N1), –97.7 ppm (α-N3). **IR**: 3114 (w), 3090 (w), 2830 (w), 1622 (s), 1588 (m), 1482(m), 1293 (m), 1278 (s), 1237 (m), 1166 (m), 818 (m), 763 (m), 752 (m), 737 (m), 689 (m) 658 (m), 519 (m), 481 cm^{-1} (m). **Elemental analysis** calcd (%) for $C_{23}H_{21}N_3O_2Zr$ (M = 462,66 g mol^{-1}): C, 59.71; H, 4.58; N, 9.08. Found: C, 57.85; H, 3.13; N, 8.01. **MS** (*m/z*, CI, *isobutene*): 877 [2 x M – OCHO$^-$], 461 [M], 416 [M – OCHO$^-$], 357 [M + H – N_2Ph], 105 [N_2Ph].

2 Details of NMR spectroscopy

2.1 NMR spectrum of complex 1

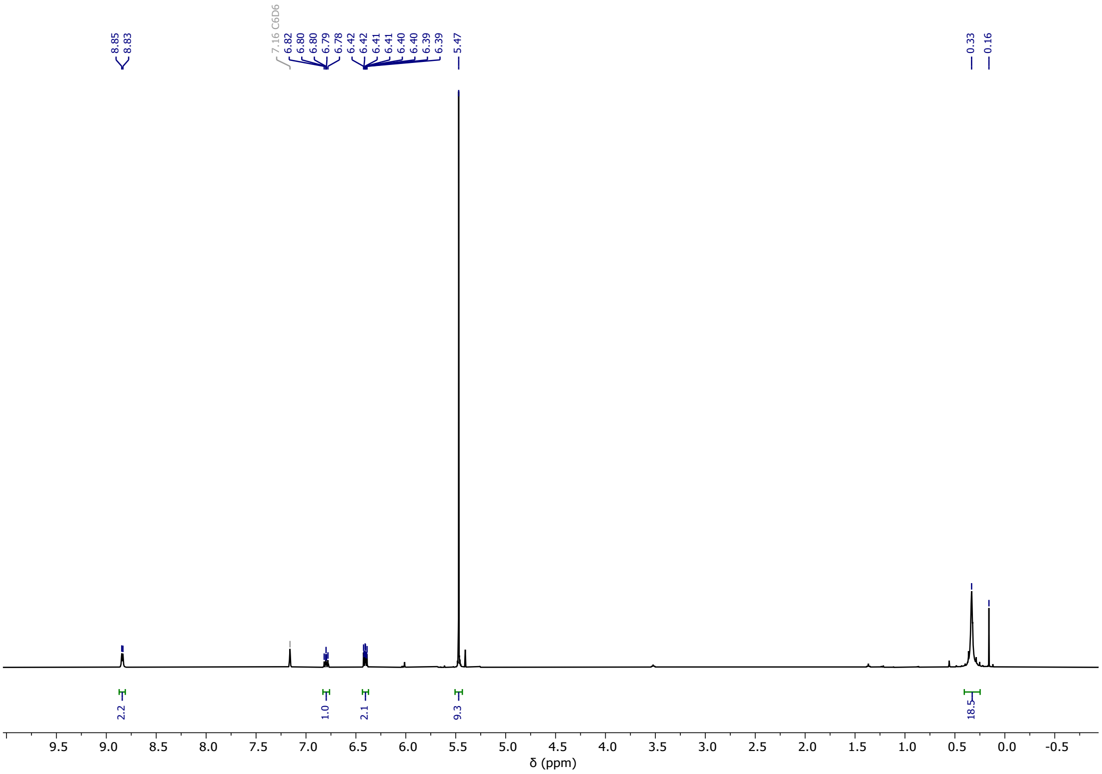

Figure S3. ^{1}H NMR spectrum of complex **1** (25 °C, benzene-d_6, 400 MHz). The resonance at 0.16 ppm corresponds to residual (uncoordinated) $Me_3SiC_2SiMe_3$.

2.2 NMR spectra of complex 2

Note: Complex ***2*** *is only a transient species at ambient conditions. We collected a series of 1D and 2D NMR spectra at ambient temperature as well as low temperature using freshly prepared in situ samples to prove connectivity. Due to the transient natur, also follow-up product* ***3*** *and free alkyne and pyridine are present in solution.*

2.2.1 NMR spectra of complex 2 in benzene-d_6 at ambient temperature

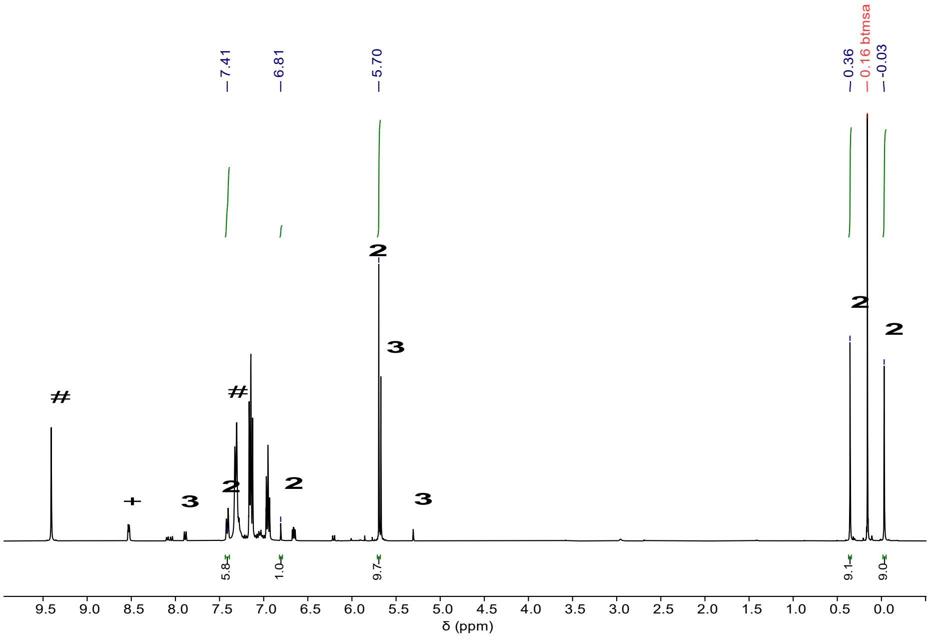

Figure S4. ^{1}H NMR spectrum of a freshly prepared sample, containing complexes **2** and **3** as the follow-up product (25 °C, benzene-d_6, 400 MHz). Selected resonances consistent with the structural motif of **2** were selected. Due to the excess of 1,3-diphenyltriazine (#) and stoichiometric amounts of free pyridine (+) and $Me_3SiC_2SiMe_3$ (btmsa), as well as the progression of the reaction to compound **3**, the resolution is not ideal. It should be noted that it is very likely that the chemical shifts of pure isolated complex **2** will differ from those reported here.

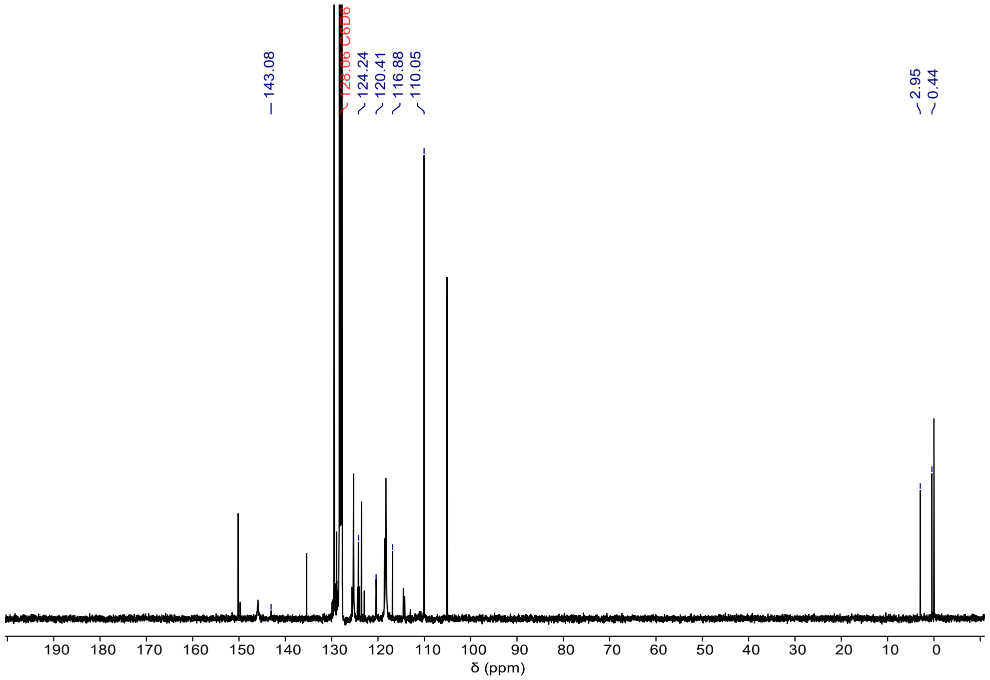

Figure S5. ^{13}C NMR spectrum of a freshly prepared sample, containing complexes **2** and **3** as the follow-up product (25 °C, benzene-d_6, 101 MHz). The characteristic α-C resonance of the vinyl group, which is expected in the low-field range, could not be detected in this experiment.

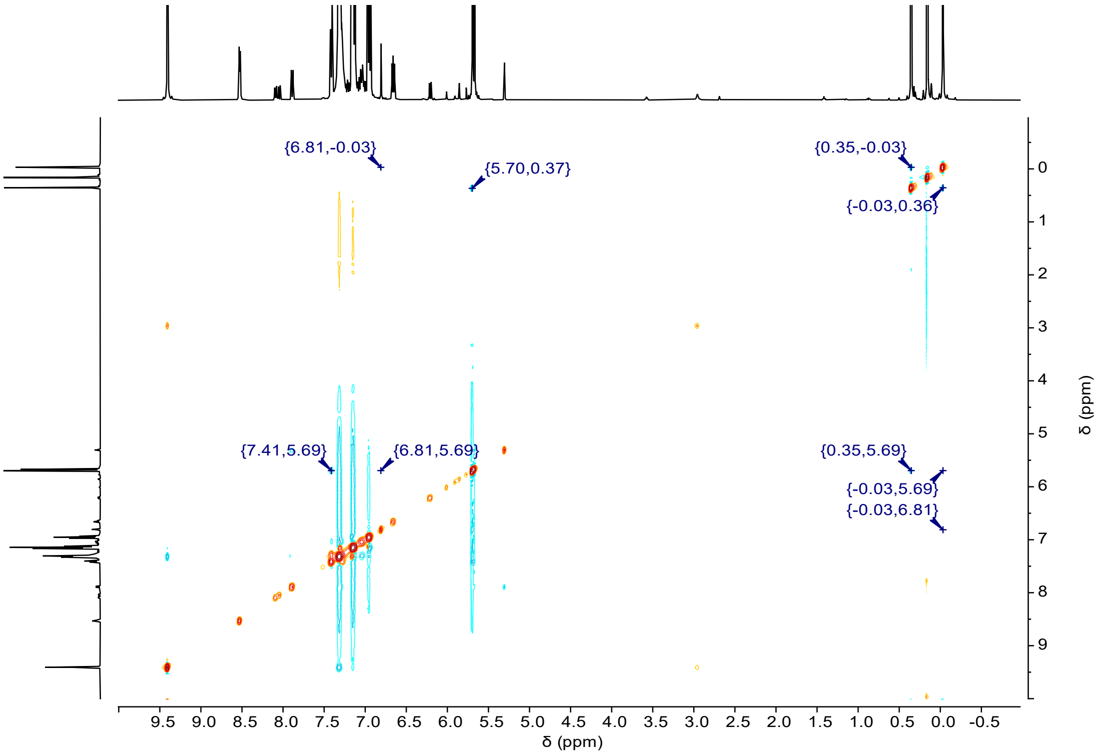

Figure S6. ^{1}H-^{1}H NOESY of a freshly prepared sample, containing complexes **2** and **3** as the follow-up product (25 °C, benzene-d_6, 400 MHz). Selected resonances/correlations support the structural motif of **2**.

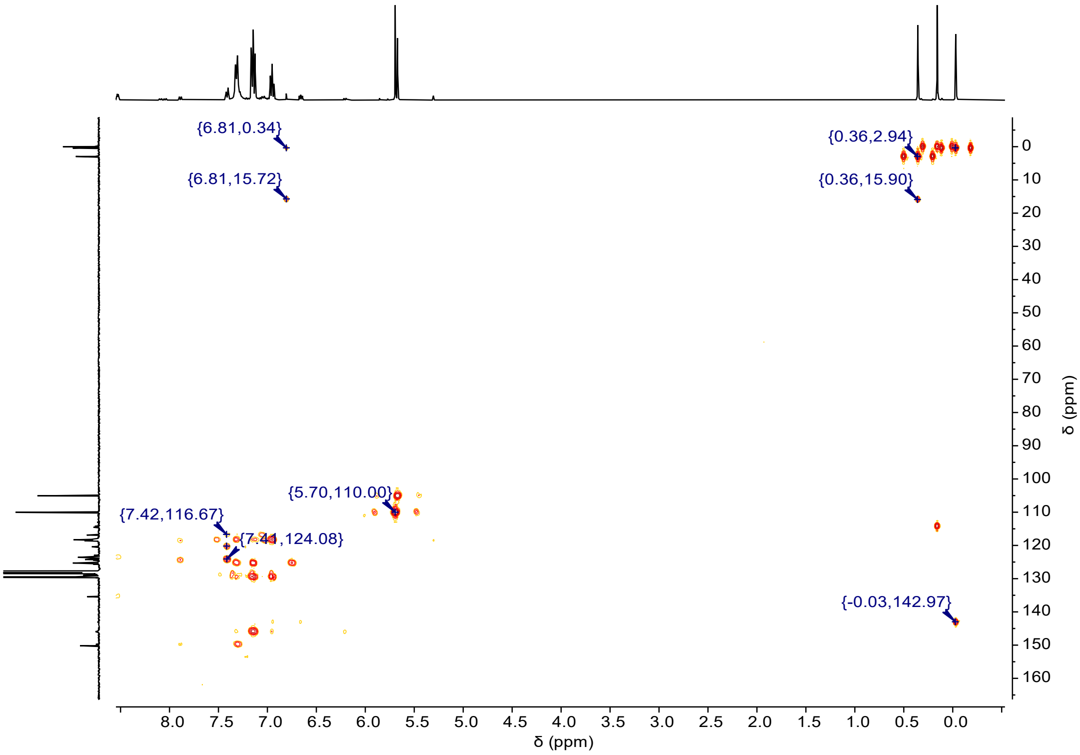

Figure S7. ^{1}H-^{13}C HMBC of a freshly prepared sample, containing complexes **2** and **3** as the follow-up product (J = 8 Hz, 25 °C, THF-d_8, 400/101 MHz). Selected resonances/correlations support the structural motif of **2**. Cross peaks at δ (^{13}C) 15.8 ppm represent the α-C of the vinyl group, they appear folded along the F1 axis. The true chemical shift is 205.4 ppm.

2.2.2 NMR spectra of complex 2 in toluene-d_8 at -20 °C

Note: The following spectra were collected from a freshly prepared sample using a 1:6 ratio of complex ***1*** *and 1,3-diphenyltriazene. After dissolving and mixing of the compounds the sample was immediately cooled to -78 °C and kept at this temperature for one week until the NMR measurement, which was performed at -20 °C. This shows that complex* ***2*** *is stable at low temperature; isolation of this species was however not successful.*

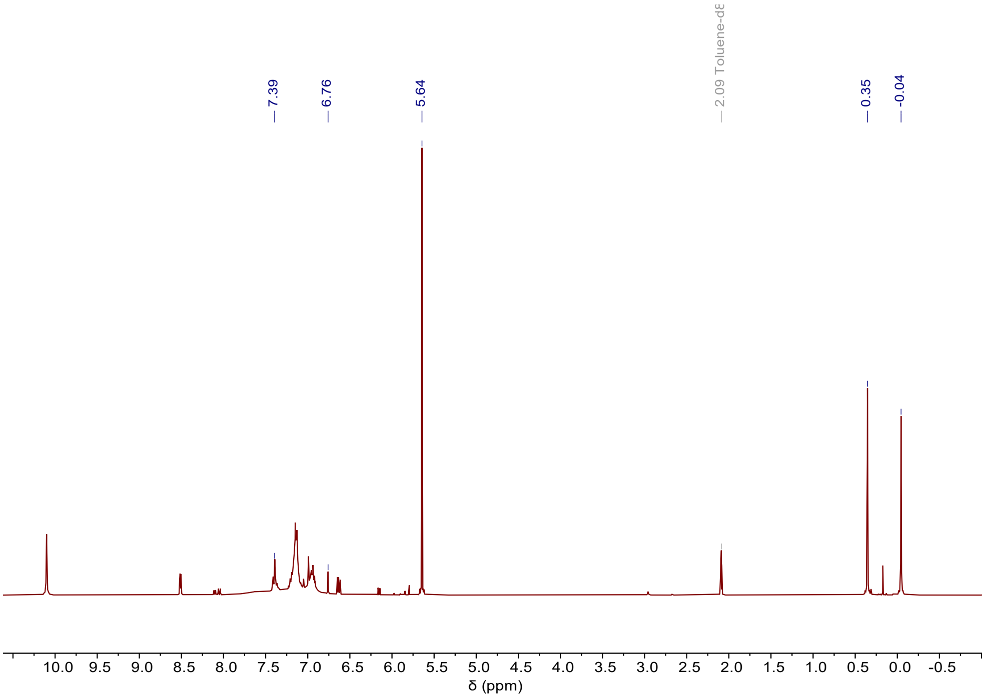

Figure S8. ^{1}H NMR spectrum of the reaction of complex **1** and 1,3-diphenyltriazene (-20 °C, toluene-d_8, 400 MHz). Selected resonances consistent with the structural motif of **2** were labeled. Signals corresponding to phenyl groups could not be further analysed due to molecular dynamics of excess free triazene and coordinated triazenide.

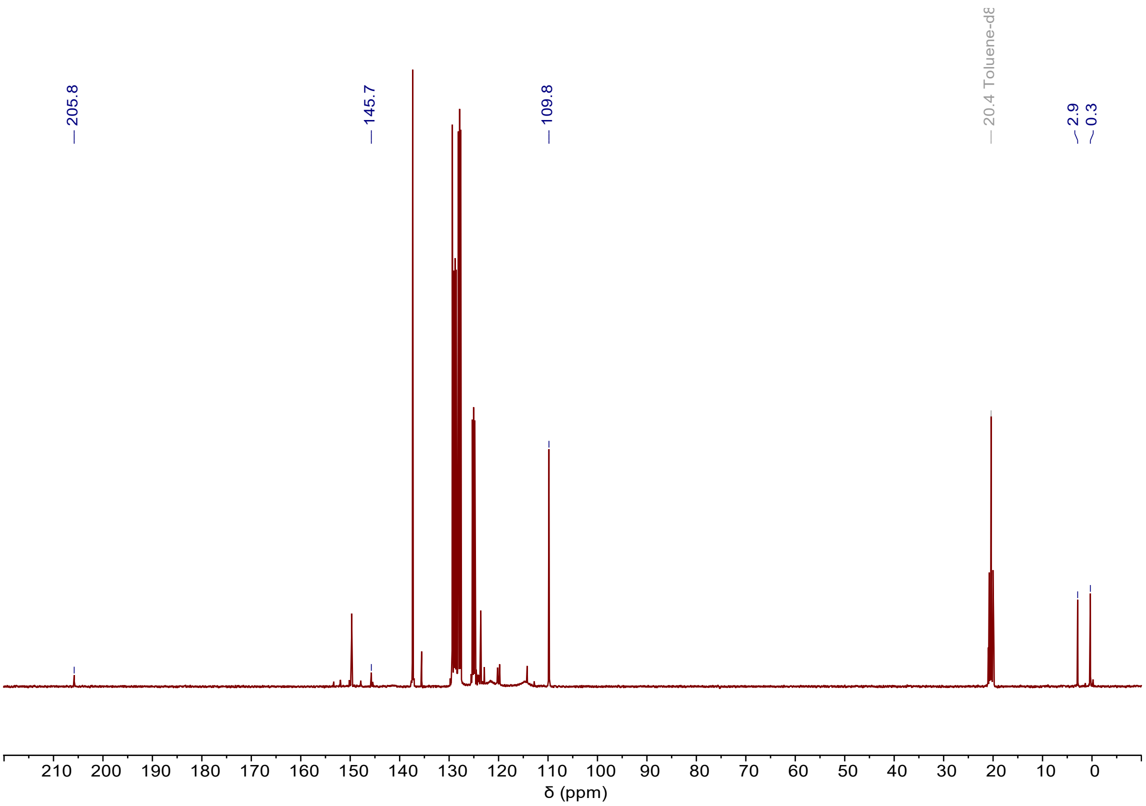

Figure S9. ^{13}C NMR spectrum of the reaction of complex **1** and 1,3-diphenyltriazene (-20 °C, toluene-d_8, 101 MHz). Characteristic resonances consistent with the structural motif of **2** are labeled. Signals corresponding to phenyl groups could not be further analysed due to molecular dynamics of excess free triazene and coordinated triazenide.

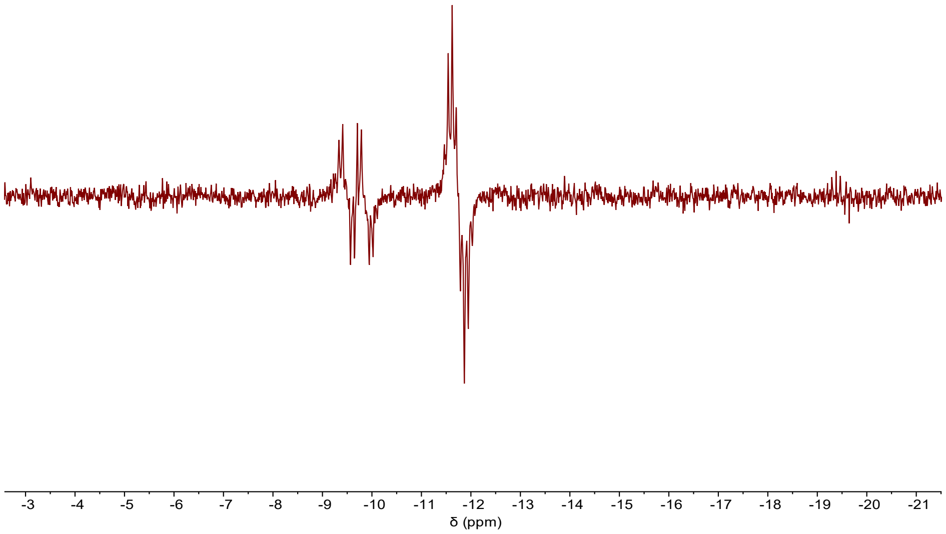

Figure S10. ^{29}Si inept spectrum of the reaction of complex **1** and 1,3-diphenyltriazene (J = 7 Hz, -20 °C, toluene-d_8, 79 MHz). The spectrum shows the two signals of the non-equivalent Me$_3$Si groups of the vinyl group, with the signal at δ -9.7 ppm corresponding to α-CSiMe$_3$ due to its additional $^3J_{Si,H}$ = 23 Hz coupling to the *trans*-C$_\beta$-H vinyl moiety. This assignment is supported by NOESY coupling. Furthermore, the signal of Me$_3$Si groups of Me$_3$SiC$_2$SiMe$_3$ (δ -19.5 ppm) is present which is explained by the follow-up reaction to complex **3**.

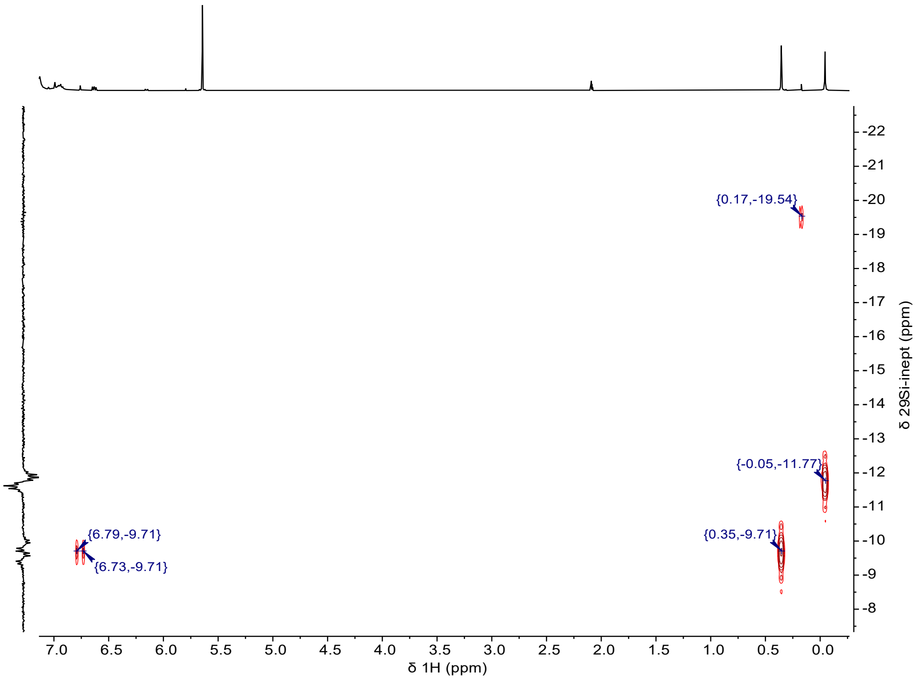

Figure S11. ^{1}H-^{29}Si HMBC spectrum of the reaction of complex **1** and 1,3-diphenyltriazene (J = 8 Hz, -20 °C, toluene-d_8, 400/79 MHz). The $^3J_{H,Si}$ satellites of the *trans*-C$_\beta$-H signal at δ (^{1}H) 6.75 ppm support the proposed structure of complex **2** containing a vinyl unit. Furthermore, the signal of Me$_3$Si groups of Me$_3$SiC$_2$SiMe$_3$ is present which is explained by the follow-up reaction to complex **3**.

2.3 NMR spectra of compound 3

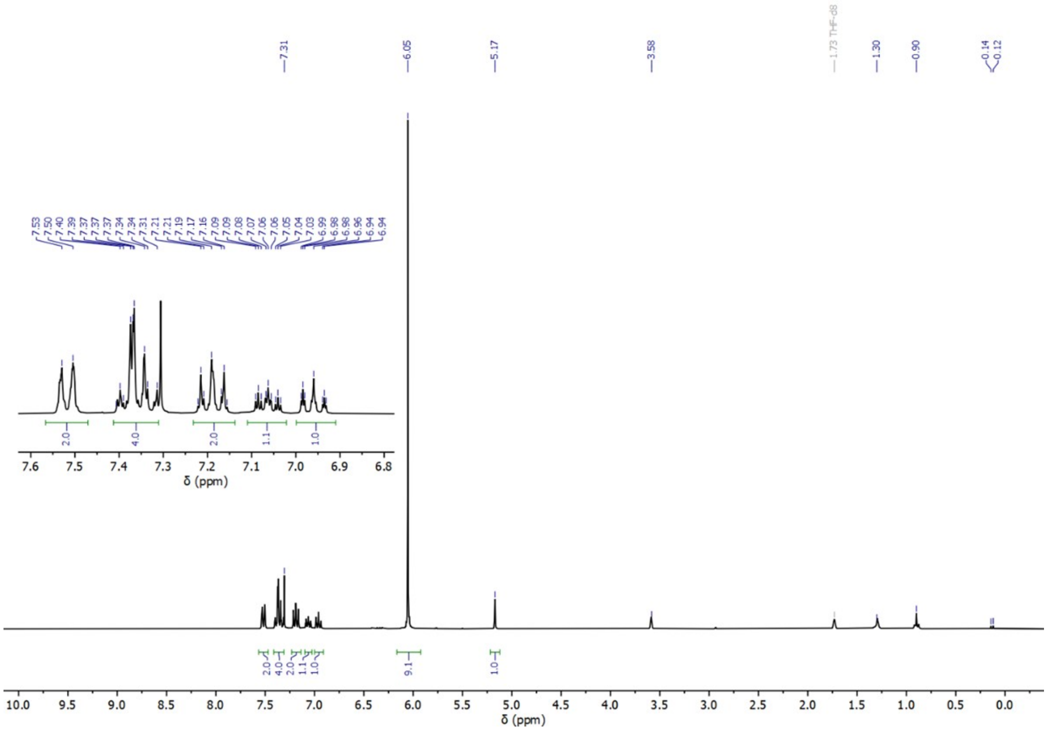

Figure S12. ^{1}H NMR spectrum of complex **3** (25 °C, THF-d_8, 300 MHz). Identified contaminants: 0.12 (s, silicone grease), 0.14 (s, free $Me_3SiC_2SiMe_3$), 0.90 (t, pentane), 1.30 (m, pentane), 1.73 (m, THF), 3.58 (m, THF), 7.31 (s, benzene).

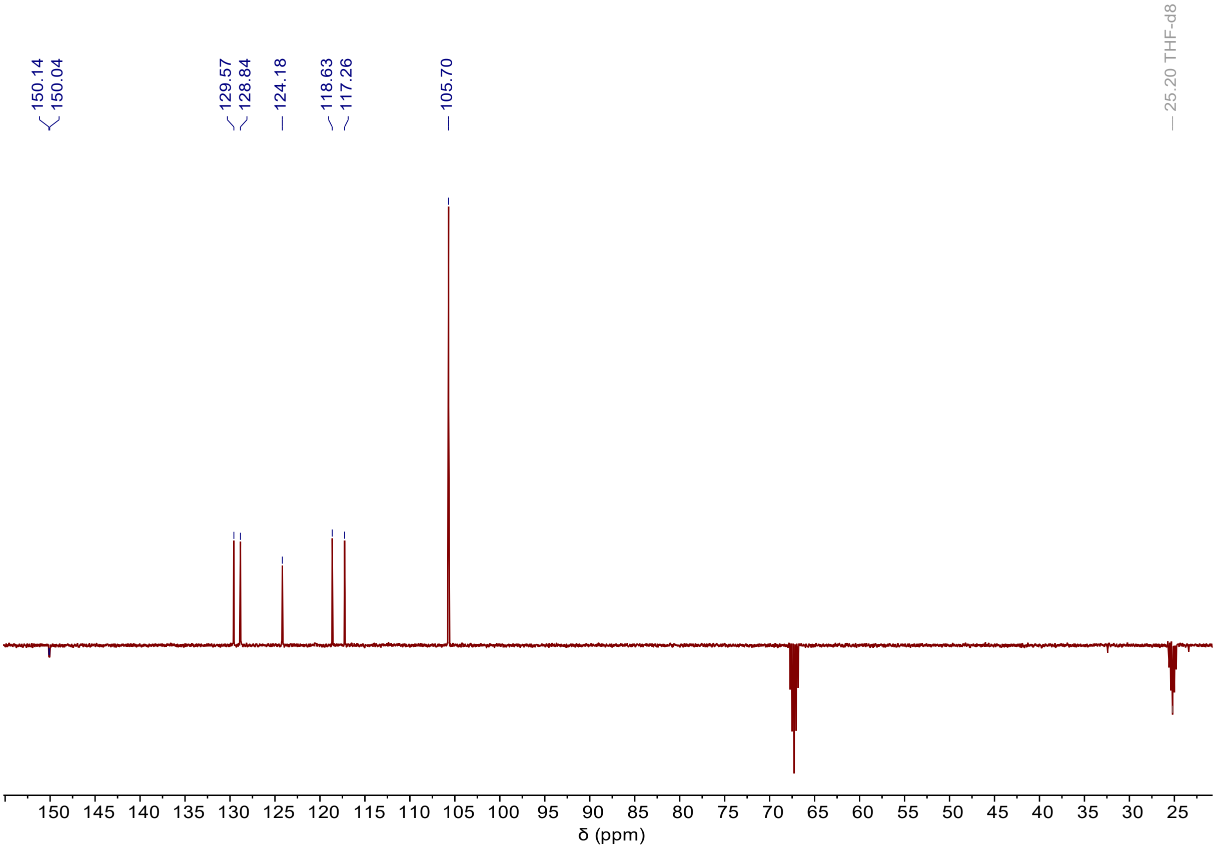

Figure S13. APT-^{13}C NMR spectrum of complex **3** (25 °C, THF-d_8, 101 MHz).

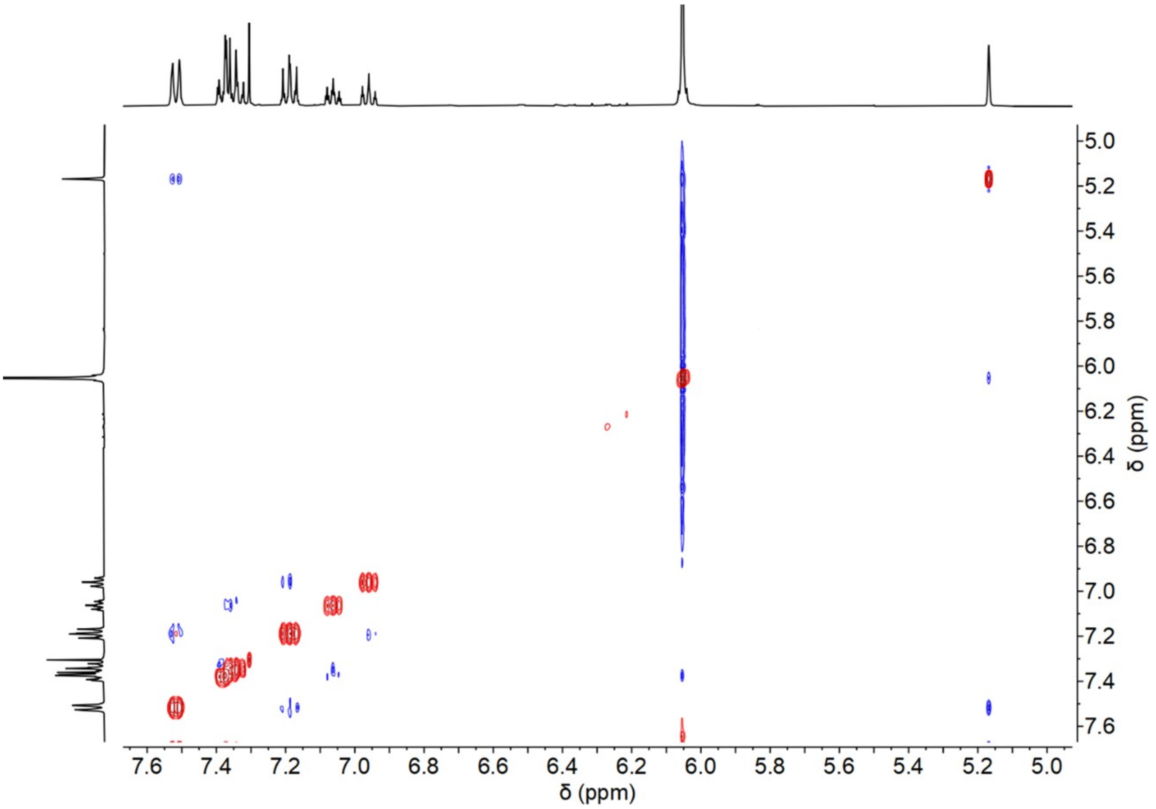

Figure S14. ^{1}H-^{1}H NOESY spectrum of complex **3** (25 °C, THF-d_8, 400 MHz).

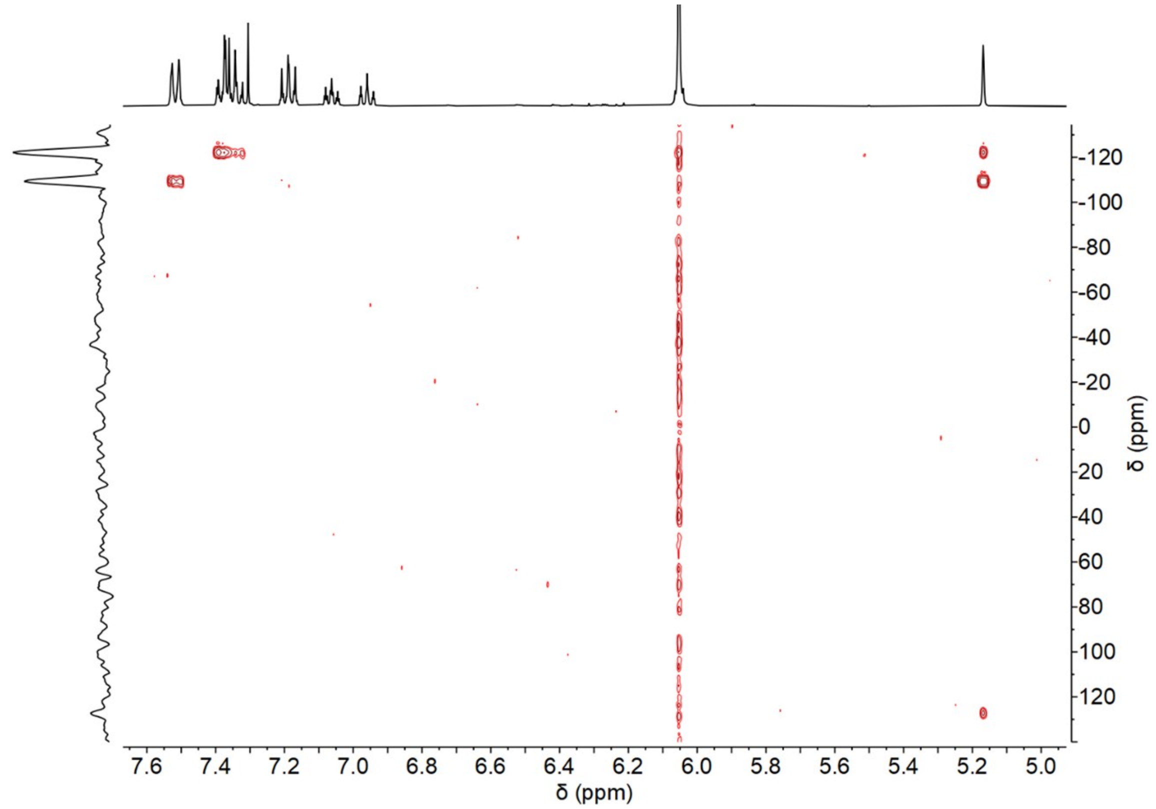

Figure S15. ^{1}H-^{15}N HMBC spectrum of complex **3** (J = 3 Hz, 25 °C, THF-d_8, 400/41 MHz). A minor correlation signal between the Cp protons (6.05 ppm) and N3 (–122.5 ppm) is also present, in this Figure obscured by t_1 noise. $^2J_{\mathrm{N,H}}$ N1/Zr-H is in the range 4-5 Hz and $^3J_{\mathrm{N,H}}$ N1/*ortho*-H is about 4 Hz.

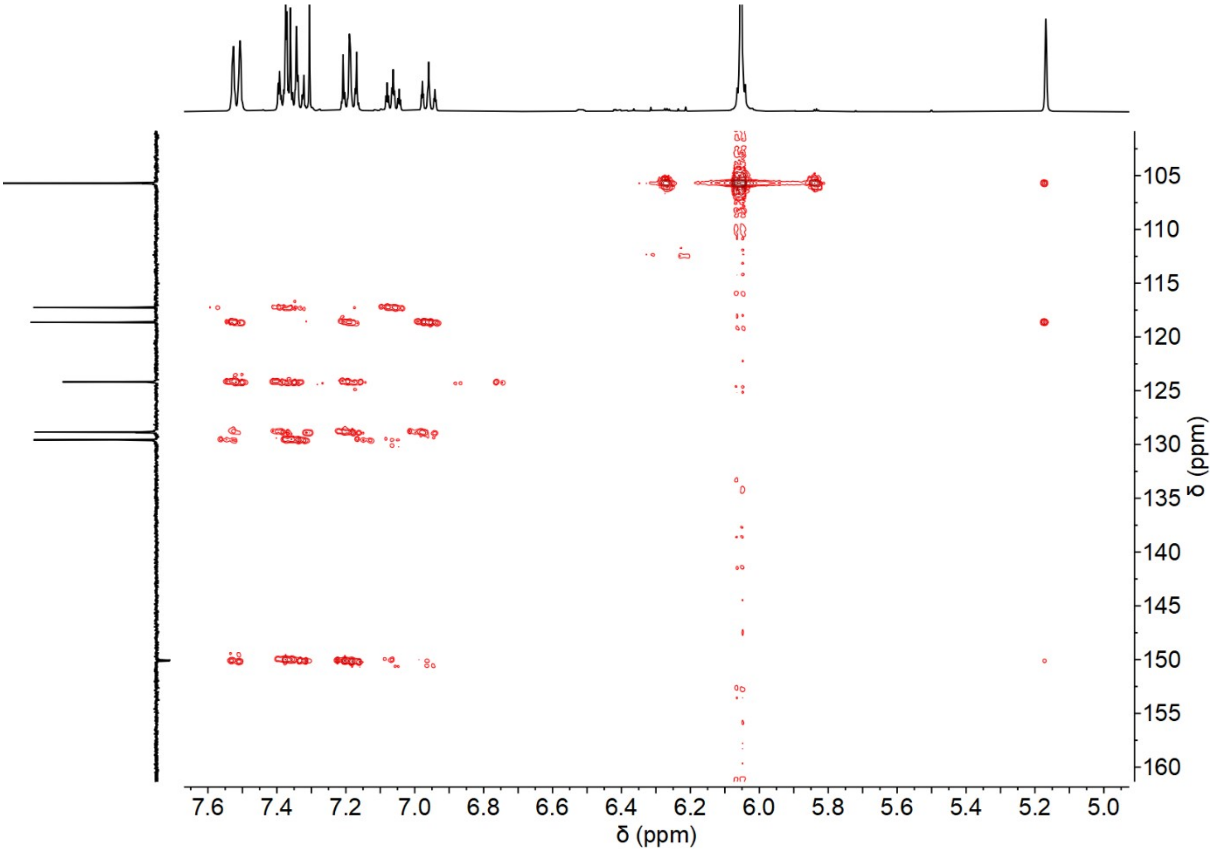

Figure S16. ^{1}H-^{13}C HMBC spectrum of complex **3** (J = 8 Hz, 25 °C, THF-d_8, 400/101 MHz).

2.4 NMR spectra of complex 4

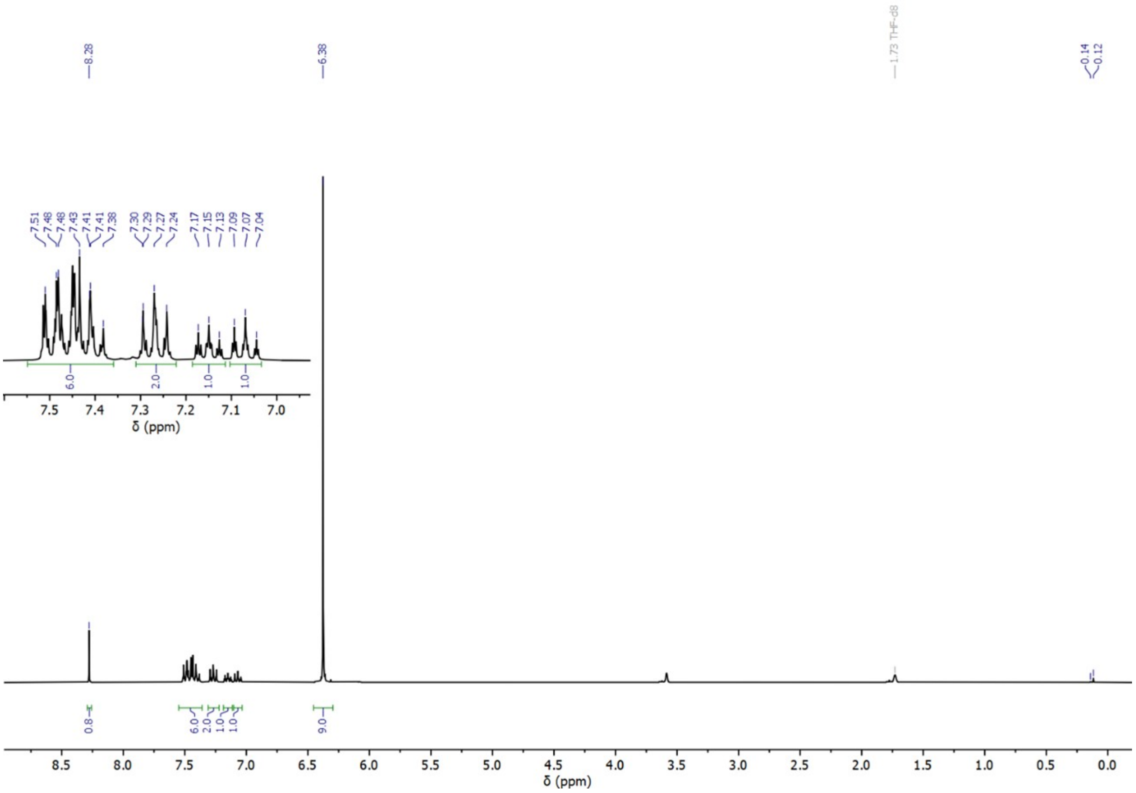

Figure S17. ^{1}H NMR spectrum of complex **4** (25 °C, THF-d_8, 300 MHz).

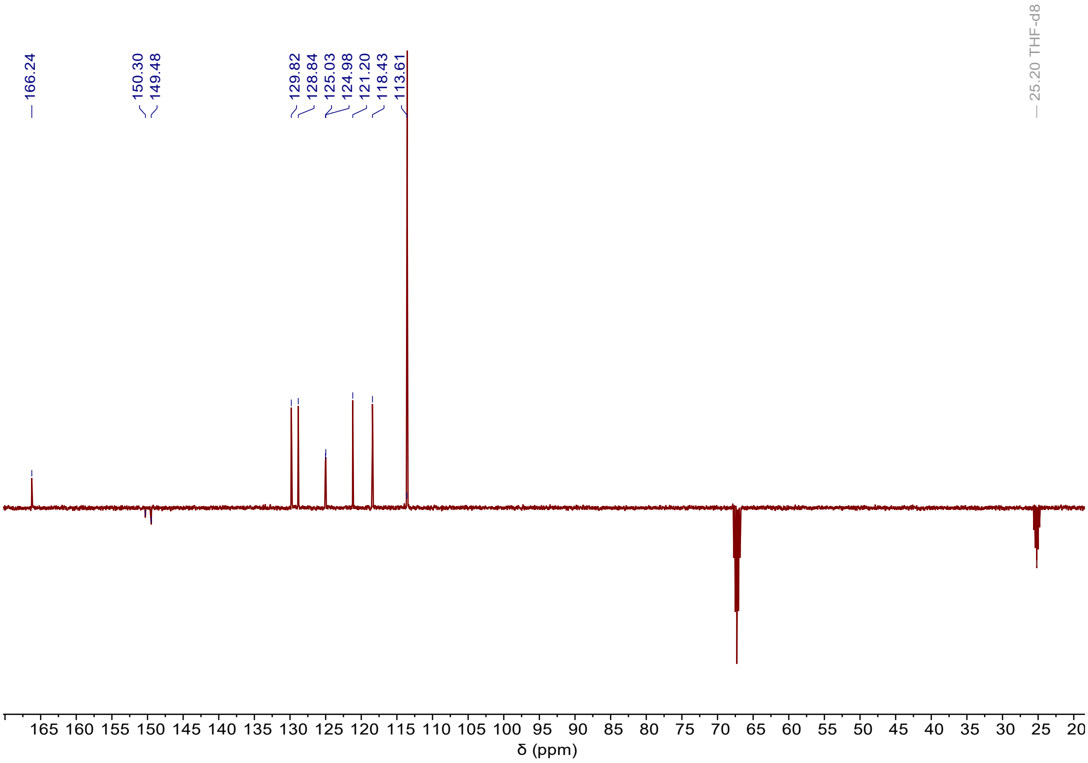

Figure S18: APT-^{13}C NMR spectrum of complex **4** (25 °C, THF-d_8, 101 MHz).

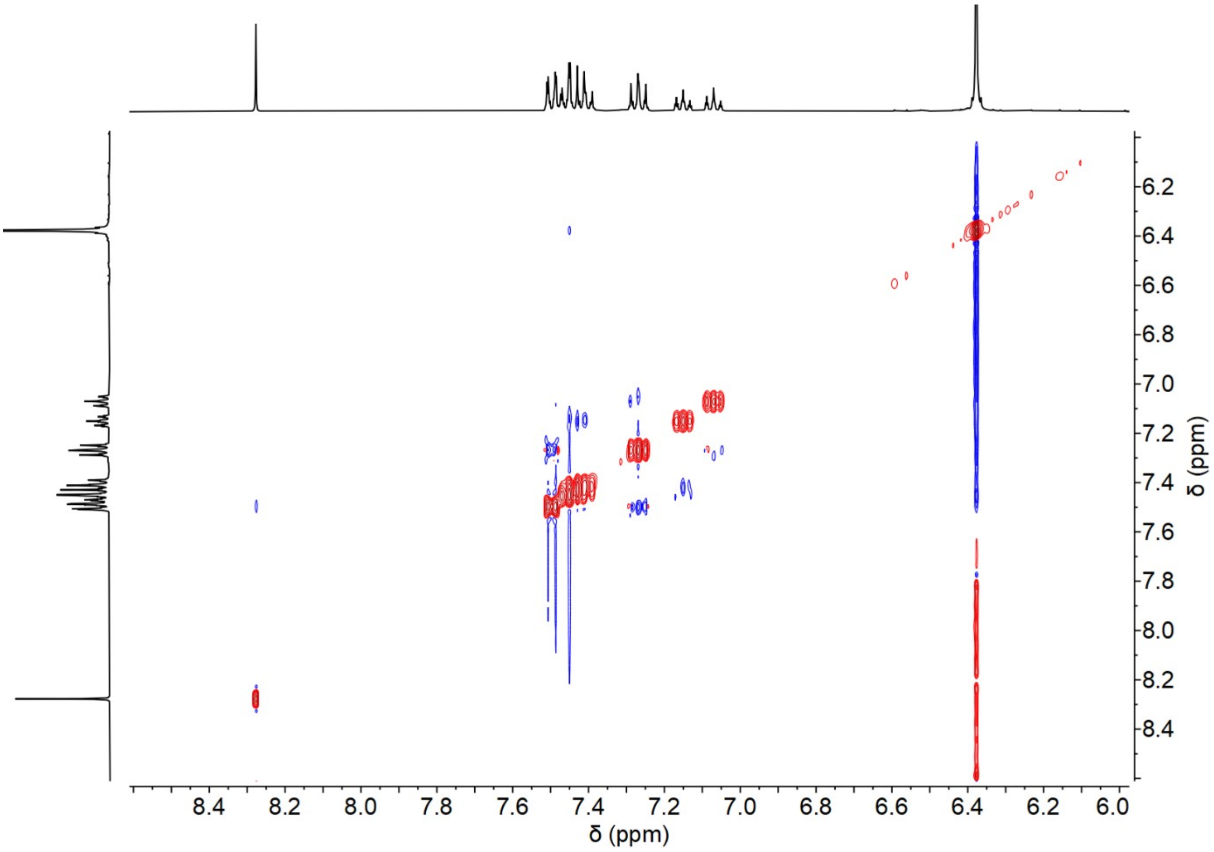

Figure S19. ^{1}H-^{1}H NOESY spectrum of complex **4** (25 °C, THF-d_8, 400 MHz).

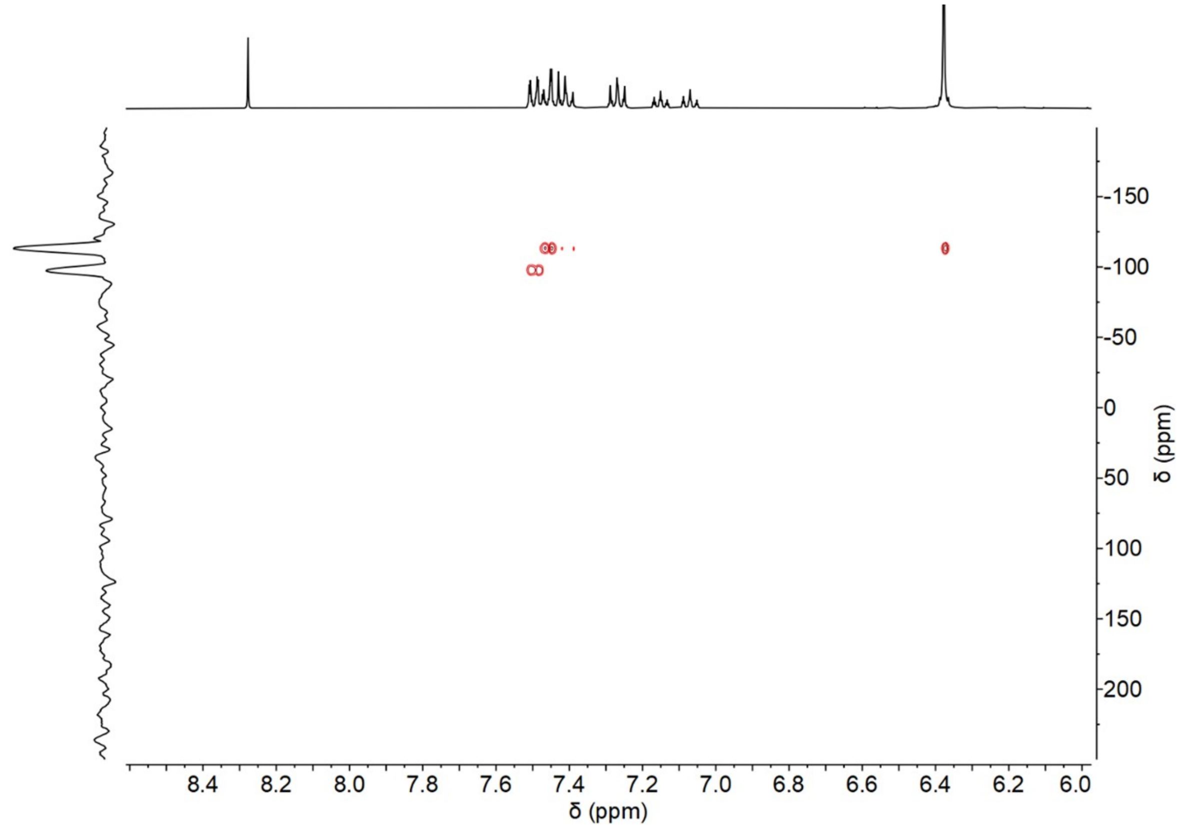

Figure S20. ^{1}H-^{15}N HMBC spectrum of complex **4** (J = 2 Hz, 25 °C, THF-d_8, 400/41 MHz). $^3J_{N,H}$ N1/*ortho*-H and N3/*ortho*-H both are about 4 Hz. A correlation signal for N2 was found neither with a transfer delay optimised for 3 nor for 5 Hz.

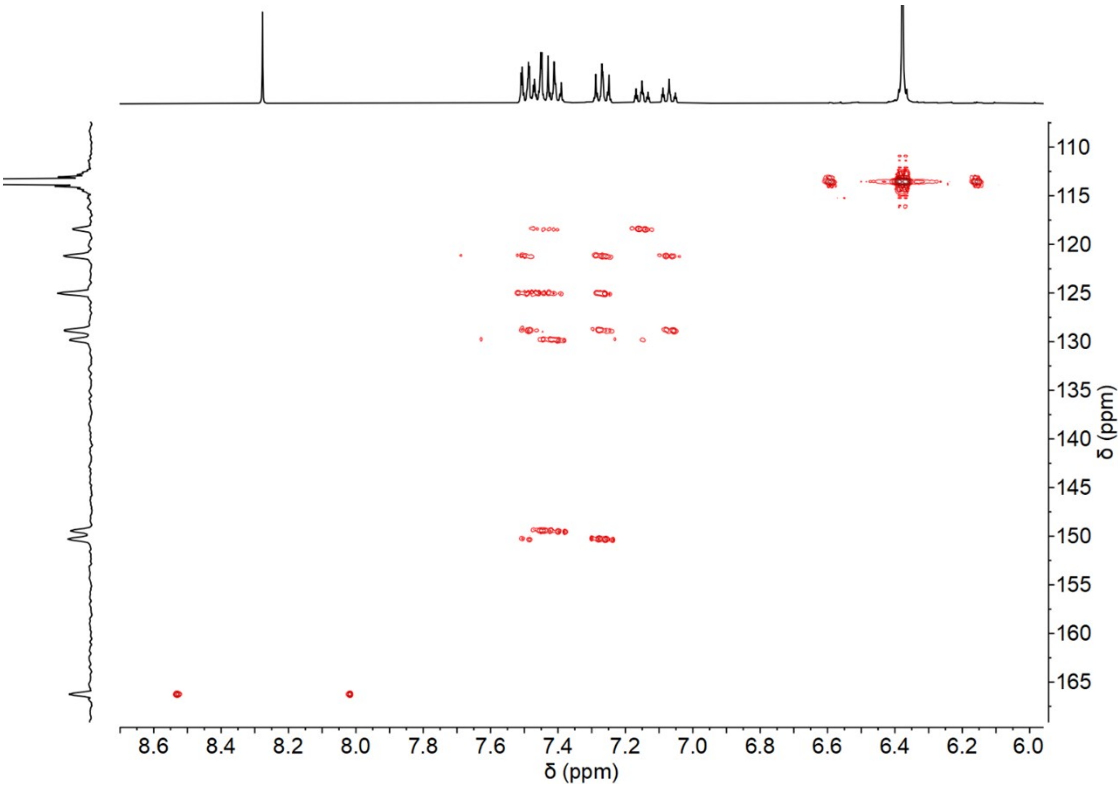

Figure S21. ^{1}H-^{13}C HMBC spectrum of complex **4** (*J* = 8 Hz, 25 °C, THF-d_8, 400/101 MHz).

2.5 Detailed analysis of the ^{15}N NMR chemical shift pattern

Note: The labeling N1/N2/N3 used here does not match the numbering used for the molecular structure plots.

For 1,3-triazenes (R–N^1=N^2–N^{3}R'R"), the central nitrogen atom shows the largest chemical shift. In general, δ(N2) > δ(N1) > δ(N3) is found with typical values of 50 to 70 ppm for N2, –40 to 0 ppm for N1, and –220 to –200 ppm for N3.[9,10,11] For R' = H, only a single, averaged signal is observed for N1 and N3 due to fast proton exchange and shift of the double bond.

Table S1. ^{15}N NMR shifts of 1,3-diphenyltriazene (R = R" = Ph, R' = H) and its complexes.

Entry	δ(N1)	δ(N2)	δ(N3)	Comment	Reference
1	–100.5	61.6	–100.5	At 40 °C in cycloheptanone	10
2	–109.3		–109.3	Averaged data computed from entry 3	
3	–20.5	?	–198.0	At –90°C in dichloromethane	11
4	–15.6	?	–199.2	Os complex with neutral triazene (R' = H) at –90 °C in dichloromethane	11
5	–107.4		–107.4	Averaged data computed from entry 4	
6	–140.0	?	–140.0	Ru complex with triazenide (no R')	11
7	–122.5	126.2	–109.6	Zr-H complex **3** with triazenide (no R')	This work
8	–113.3	Not found	–97.7	Zr formate complex **4** with triazenide (no R')	This work

Upon complexation of the 1,3-triazene as neutral ligand with monodentate κ^1-N coordination, a minor increase in the chemical shift is found (Table S1, entries 3 *vs.* 4 and entries 2 *vs.* 5, respectively). This effect is stronger and of opposite direction for N1 and N3 if the triazene is deprotonated to form a bidentate κ^2-N,N triazenide ligand (Table, entries 3 *vs.* 6/7/8). The similarity of shifts observed for N1 and N3 reflects the delocalisation of π electrons and the resulting leveling of the NN bond lengths (Figure 3 in the manuscript). In complexes **3** and **4**, the triazenide is in an unsymmetrical environment (this is not the case for the Ru complex from entry 6) and a slight difference in the chemical shifts of N1 and N3 is observed. In accordance with the lack of symmetry, a perceptible scalar coupling between the cyclopentadienyl protons and only one of the triazenide nitrogen atoms, *viz.* N1 (opposite to the H or formate group), is observed (Figures S11 and S16). A large "coordination shift" occurs even for N2, although there is no direct Zr-N interaction and "coordination shift" might be not the appropriate term. The effect might rather originate from an increase in chemical shift anisotropy caused by the special bonding situation.

3 Crystallographic details

Table S2. Crystallographic details of complexes **3** and **4**.

	3	**4**
Chem. Formula	$C_{49.50}H_{51}N_6Zr_2$	$C_{23}H_{21}N_3O_2Zr$
Form. weight [g mol^{-1}]	912.40	462.65
Colour	orange	yellow
Cryst. system	monoclinic	monoclinic
Space group	$P2_1/n$	$P2_1/n$
a [Å]	18.1865(10)	13.9161(7)
b [Å]	11.1064(6)	11.0704(6)
c [Å]	21.3125(12)	14.3592(7)
α [°]	90	90
β [°]	99.3567(11)	115.420(2)
γ [°]	90	90
V [Å^3]	4247.6(4)	1997.96(18)
Z	4	4
$\rho_{calc.}$ [g cm^{-3}]	1.427	1.538
μ [mm^{-1}]	0.533	4.706
T [K]	110(2)	150(2)
radiation type	MoKα	CuKα
reflections measured	54414	11598
independent reflections	10249	3374
observed reflections with $I > 2\sigma(I)$	8770	3299
$R_{int.}$	0.0361	0.0230
F(000)	1880	944
R_1 ($I > 2\sigma(I)$)	0.0421	0.0223
wR_2 (all data)	0.1027	0.0566
GOF on F^2	1.028	1.055
Parameters	549	266
CCDC number	2342475	2342476

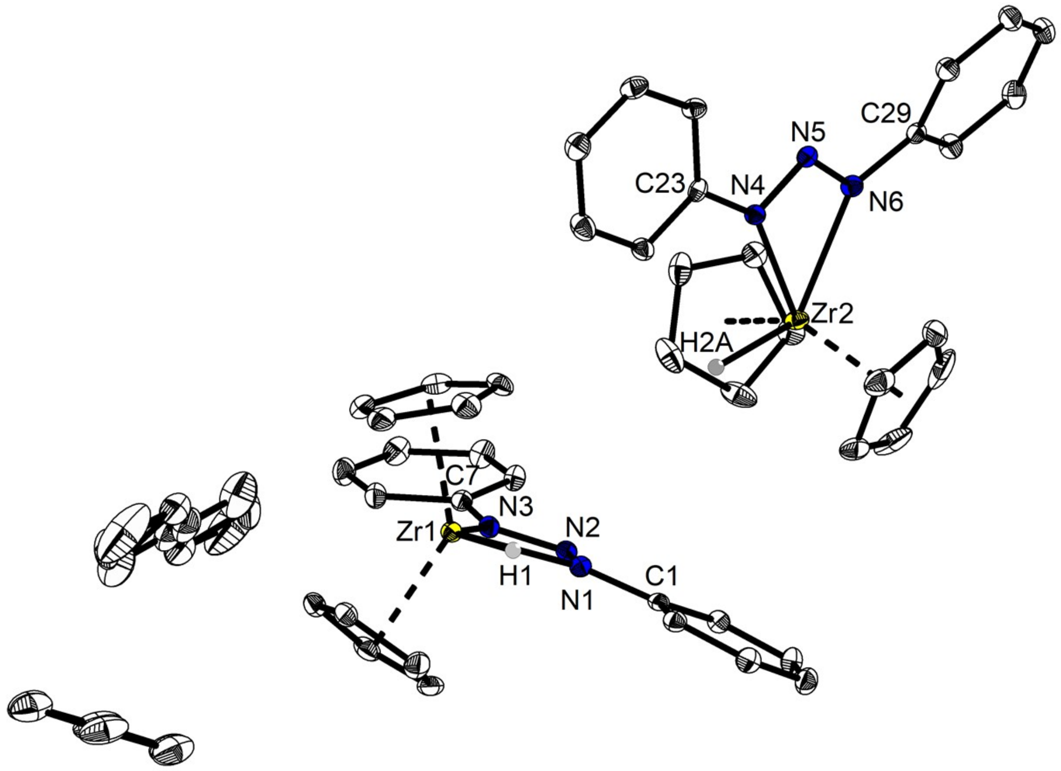

Figure S22. Illustration of the full asymmetric unit of complex **3**. The asymmetric unit shows a second molecule of complex **3** and co-crystallised solvent molecules benzene (bottom left) and pentane (disordered, left). Crystallographic details can be found in the corresponding crystallographic information file (cif).

4 Details of vibrational spectroscopy

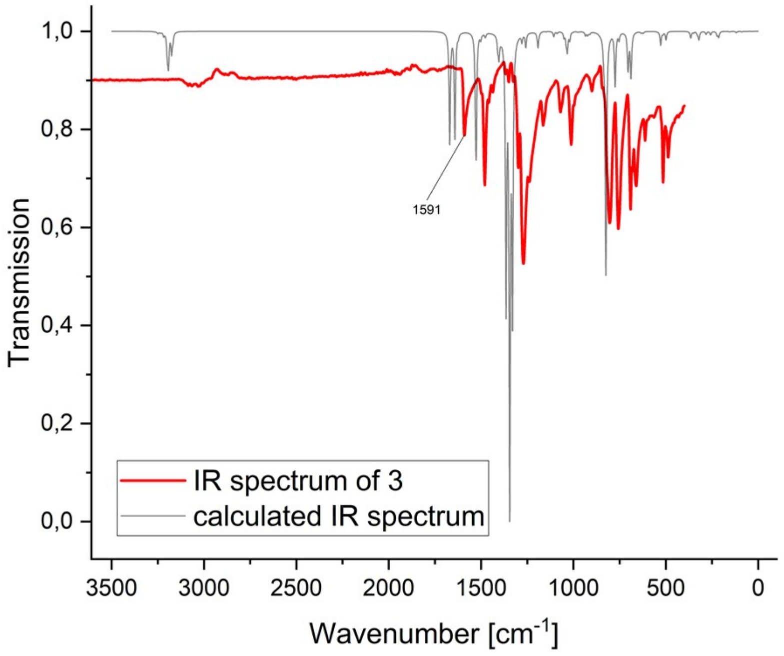

Figure S23. Experimental and uncorrected calculated IR spectra of complex **3** (B3LYP-D3/def2-TZVP). Assignments: 3065 (sym. stretching vib. Ph-H), 3032 (asymm. stretching vib. Ph-H), 1591 (Zr-H stretching vib.) 1480 (bending vib. Ph-H), 1297 (rocking vib. Ph-H), 1271 (asym. stretching vib, N_3 and bending vib. Ph-H), 1237 (asym. stretching vib. diphenyltriazene), 802 (wagging vib. Cp-H and Zr-H), 758 and 690 (wagging vib. Ph-H), 658 cm^{-1} (bending vib. Ph-C).

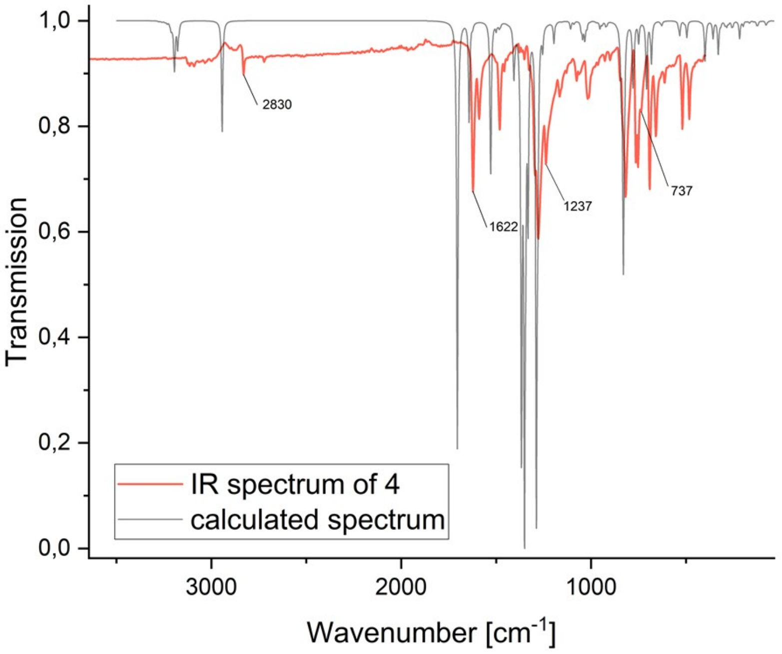

Figure S24. Experimental and uncorrected calculated IR spectra of complex **4** (B3LYP-D3/def2-TZVP). Assignments: 3114 and 3090 (asym. stretching vib. C^{Ph}-H), 2830 (stretching vib. $C^{formate}$-H), 1622 (C=O stretching vib.), 1588 and 1482 (sym. stretching vib. C^{Ph}), 1293 (asym. stretching vib. N and C^{Ph}), 1278 (bending vib. Ph-H), 1237 (stretching vib. O-$C^{formate}$), 1166 (bending vib. Ph-H), 818 (wagging vib. Cp-H), 763 and 752 (wagging vib. Ph-H), 737 (bending vib. O-C=O), 689 (wagging vib. Ph-H) 658 (bending vib. C^{Ph} and N_3), 519 (wagging vib. Ph-H), 481 cm^{-1} (bending vib. N-C^{Ph}).

5 NMR stability/reactivity tests of complexes 3 and 4

5.1 Stability of 4 towards hydrogen

Complex **4** (15 mg) was added to a Young-NMR tube and dissolved in 0.6 mL of benzene-d_6. This mixture was degassed, and the Ar atmosphere was replaced by a atmosphere of H_2. A series of ^{1}H NMR spectra were then recorded to study the possible formation of formic acid and complex **3**. No reaction was observed at room temperature, after stepwise heating to 80 °C (for about 20 h each) or after ultrasonic treatment. This led to further experiments see below.

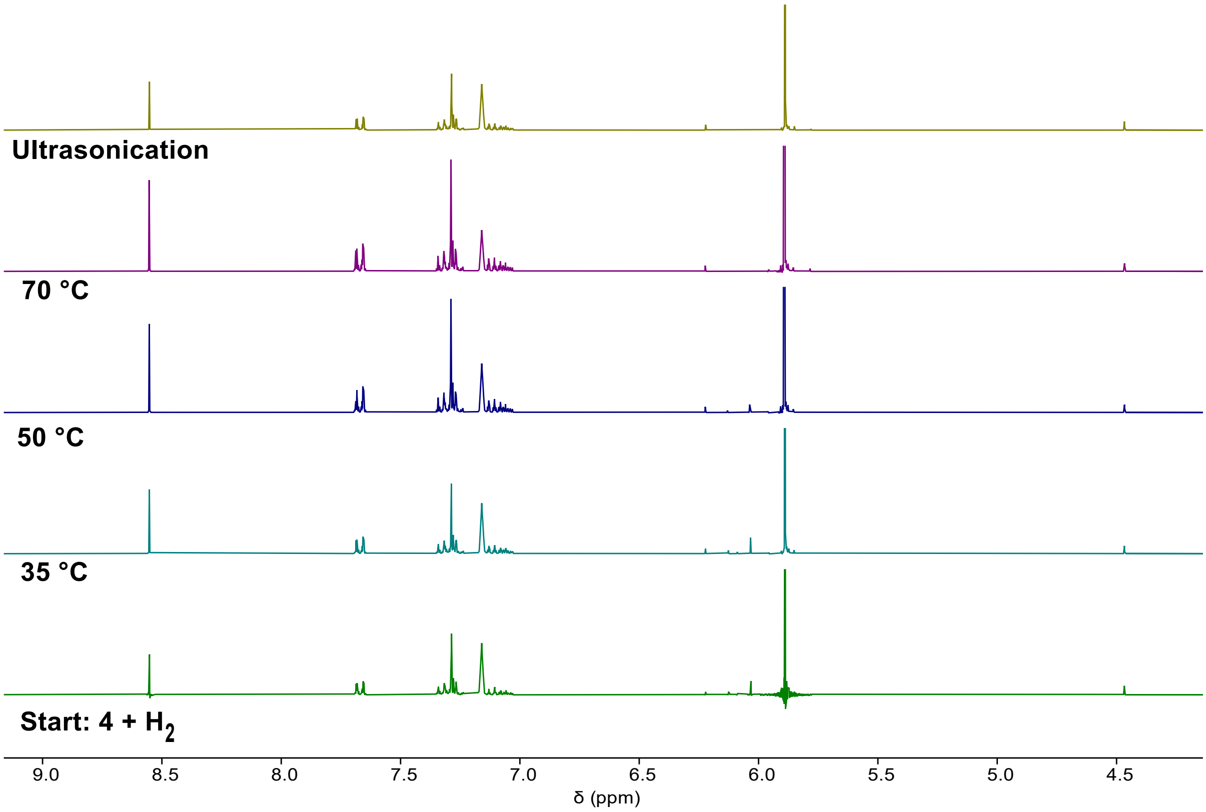

Figure S25. ^{1}H NMR spectra (25 °C, 80 MHz, benzene-d_6) of complex **4** in the presence of hydrogen (δ 4.47 ppm).

5.2 Stability of complexes 3 and 4 towards formic acid

14 mg of **3** and 13.5 mg of **4** were placed in two separate NMR tubes and 0.6 mL of a solution of 1.5 mL THF-d_8 and 34 µL of formic acid was added to each tube. As the formic acid was not well soluble in THF and some precipitation occurred, the exact equivalents added cannot be determined, but an NMR spectrum of the saturated formic acid/THF solution showed that formic acid was present in solution. The formic acid was dried over molecular sieves for three days before use. In both cases precipitation of a solid was observed, in complex **3** after keeping the NMR tube at room temperature for three days and in complex **4** after the addition of the formic acid solution.

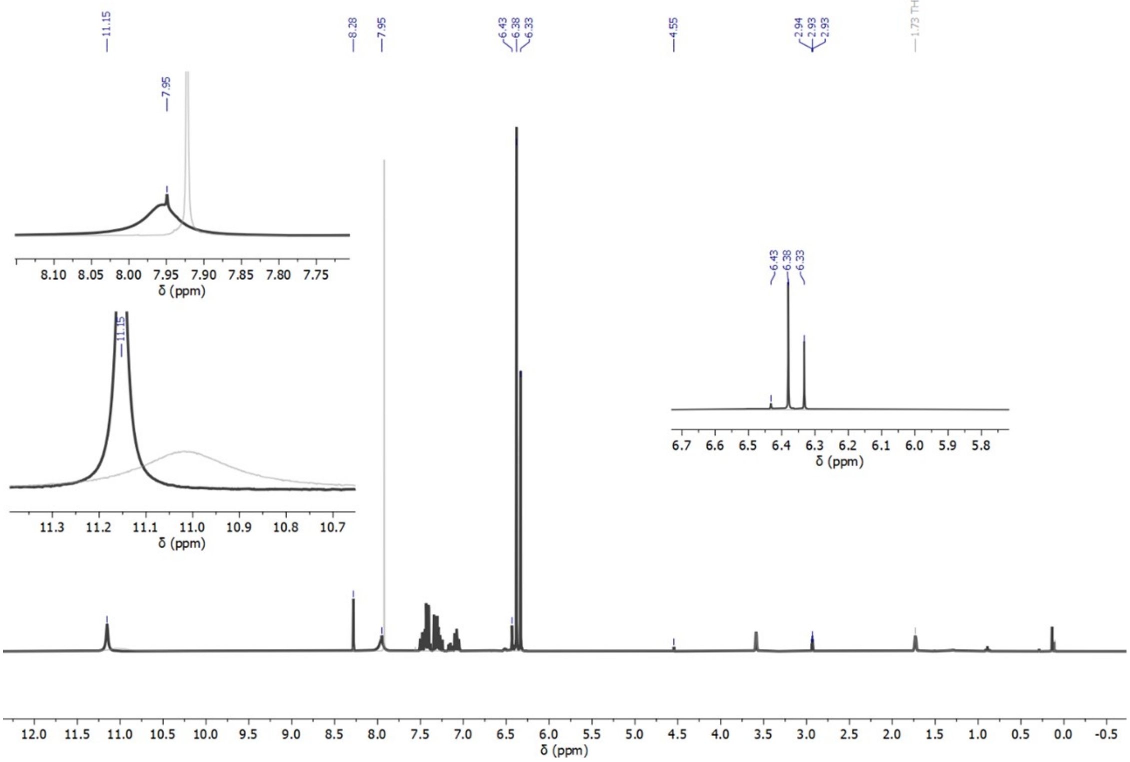

Figure S26. ^{1}H NMR spectrum (25 °C, 300 MHz, THF-*d*$_8$) of complex **3** one day after addition of formic acid in THF-*d*$_8$. The NMR spectrum of the formic acid-THF solution is shown in grey. Signals in the Cp region: δ 6.43 (unidentified), 6.38 (**4**), 6.33 (unidentified), 4.55 ppm (molecular hydrogen).

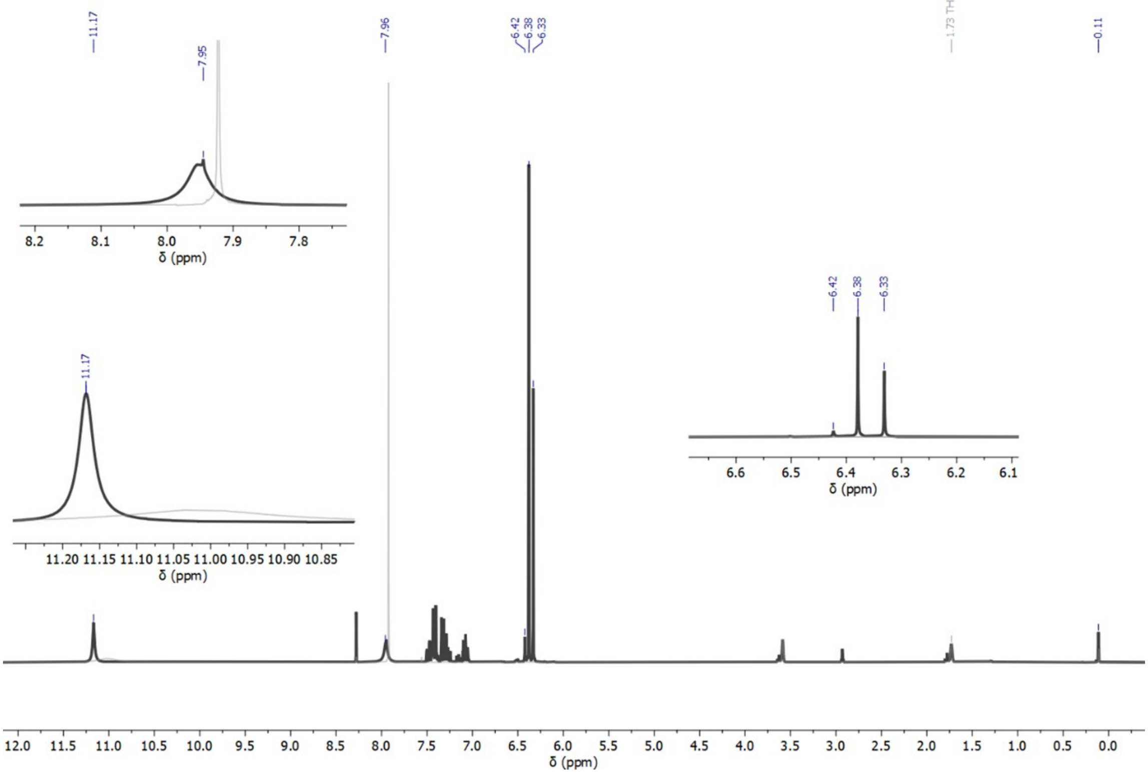

Figure S27. ^{1}H NMR spectrum (25 °C, 300 MHz, THF-*d*$_8$) of complex **4** one day after addition of formic acid in THF-d$_8$. The NMR spectrum of the formic acid-THF solution is shown in grey. Signals in the Cp region: δ 6.42 (unidentified), 6.38 (**4**), 6.33 ppm (unidentified).

5.3 Stability of complex 3 towards selected bases

Complex **3** was placed in three Young NMR tubes in a glove box and 0.6 mL of THF-d_8 and NEt_3 or pyridine or 1,8-diazabicyclo(5.4.0)undec-7-ene (DBU) were added using a Hamilton syringe (see the table below for details). ^1H NMR spectra were recorded after mixing the reagents, the solution of **3** and NEt_3 showed a small amount of black precipitate which did not appear to increase with time. After six days, during which the NMR tubes were kept at room temperature, another NMR spectrum was recorded for each sample. CO_2 was then introduced by freezing the solution using liquid nitrogen, evacuating the NMR tube, thawing, and opening the tube to a CO_2 atmosphere. NMR spectra were again recorded directly after the addition and after three days at room temperature. The formation of a dark oily substance was observed when CO_2 was added to the sample containing DBU as the base.

m(**3**) / mg	n(**3**) / mmol	Eq.(**3**)	base	V(base) / µL	n(base) / mmol	Eq. (base)
16.1	0.038	1	NEt_3	53	0.38	10
14.7	0.035	1	pyridine	28	0.35	10
15.9	0.038	1	DBU	57	0.38	10

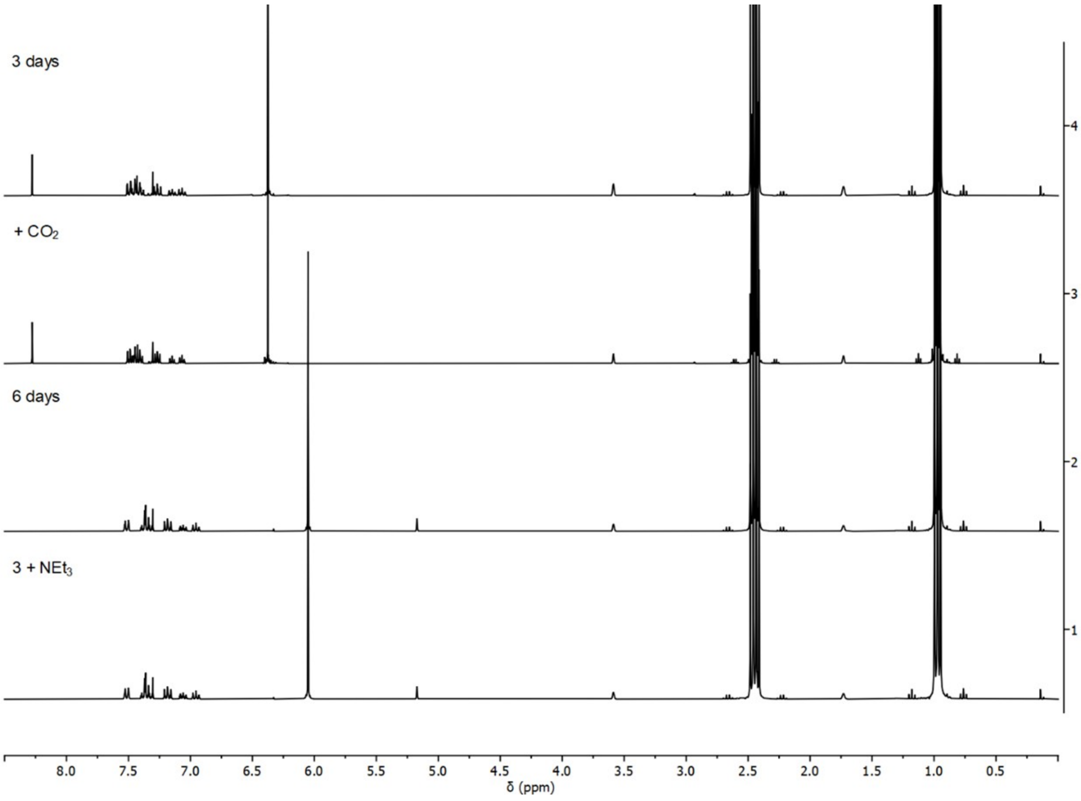

Figure S28. ^1H NMR spectrum (25 °C, 300/400 MHz, THF-d_8) of complex **3** after addition of NEt_3, after six days (NMR tube was kept at room temperature), upon addition of CO_2 and further three days at room temperature.

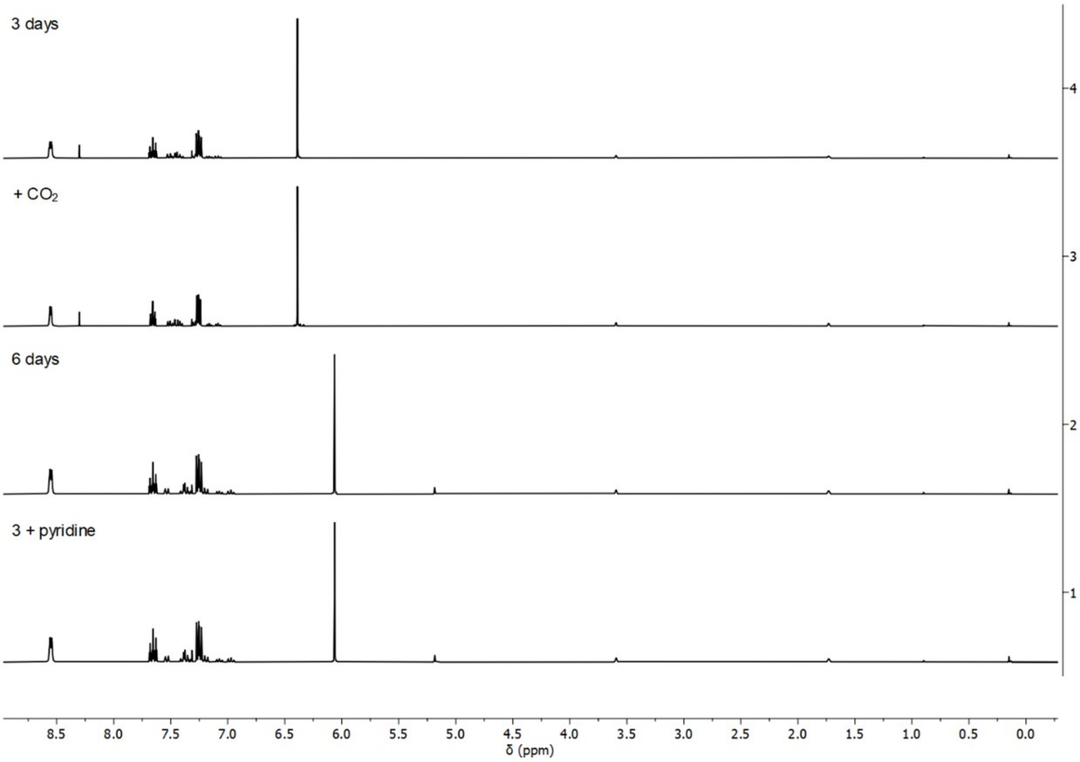

Figure S29. ^{1}H NMR spectrum (25 °C, 300/400 MHz, THF-d_8) of complex **3** after addition of pyridine, after six days (NMR tube was kept at room temperature), upon addition of CO_2 and further three days at room temperature.

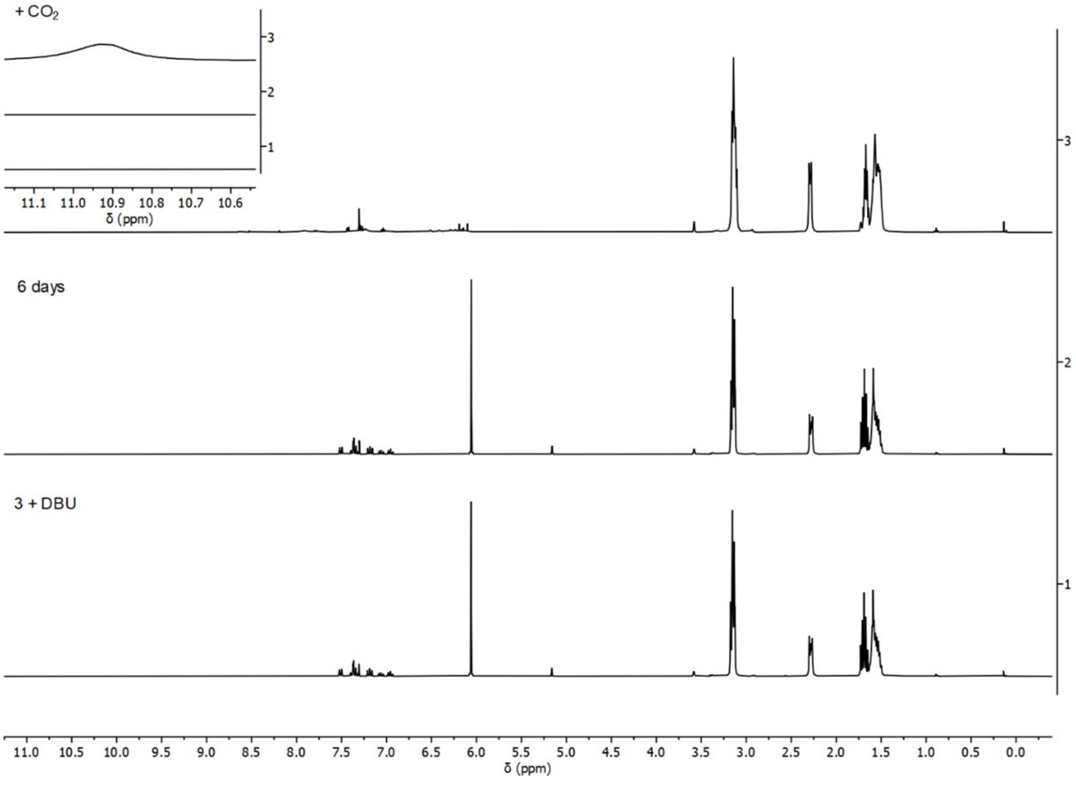

Figure S30. ^{1}H NMR spectrum (25 °C, 300/400 MHz, THF-d_8) of complex **3** after addition of DBU, after six days (NMR tube was kept at room temperature), upon addition of CO_2, due to decomposition of the sample no further spectra were recorded.

5.4 Stability of complex 4 towards selected bases

Complex **4** was added to three Young NMR tubes inside the glove box and 0.6 mL of THF-d_8 and NEt_3 or pyridine or DBU were added using a Hamilton syringe (see the table below for details).

m(**4**) / mg	n(**4**) / mmol	Eq.(**4**)	base	V(base) / µL	n(base) / mmol	Eq. (base)
14.3	0.031	1	NEt_3	43	0.31	10
15.2	0.033	1	pyridine	27	0.33	10
15.9	0.034	1	DBU	57	0.38	11.2

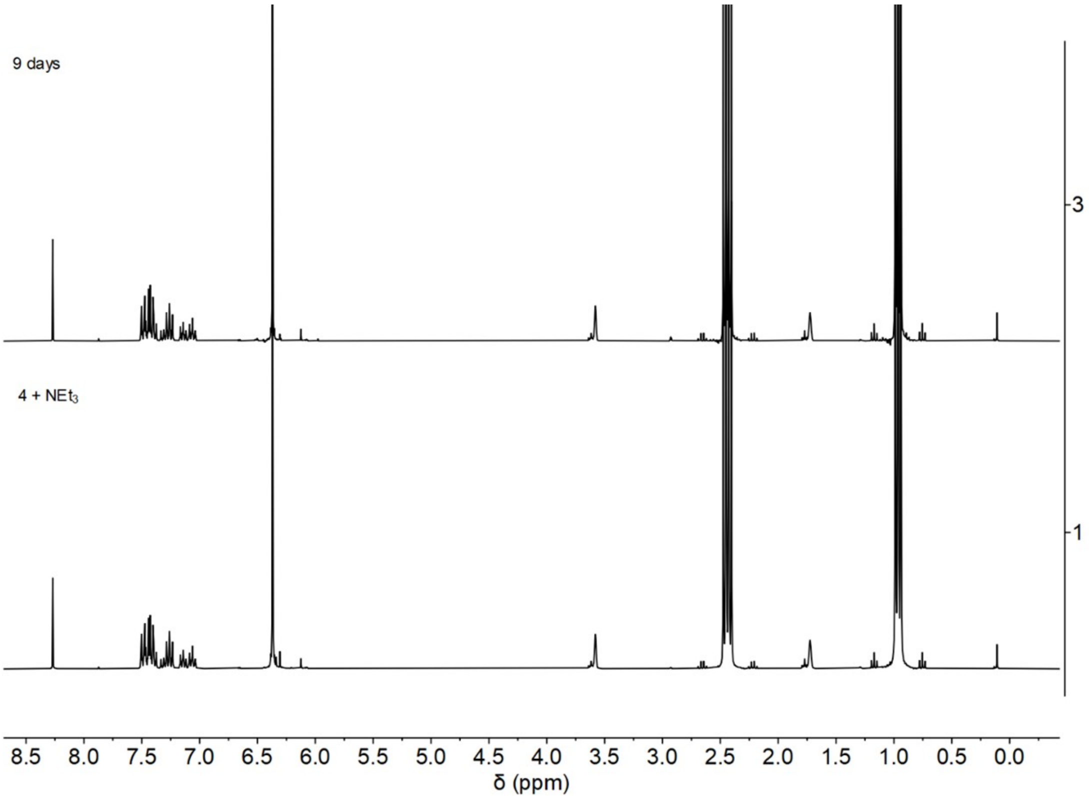

Figure S31: ^1H NMR spectra (25 °C, 300 MHz, THF-d_8) of complex **4** after addition of NEt_3, after nine days (NMR tube was kept at room temperature).

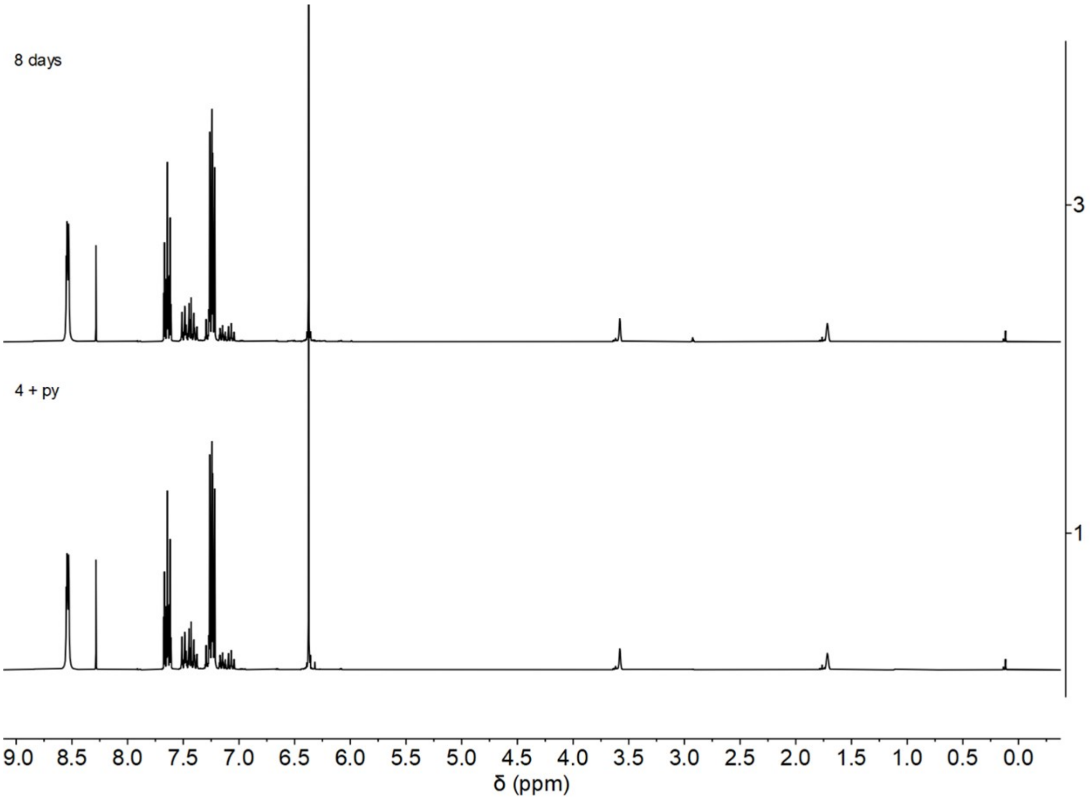

Figure S32. ^{1}H NMR spectrum (25 °C, 300 MHz, THF-d_8) of complex **4** after addition of pyridine, after eight days (NMR tube was kept at room temperature).

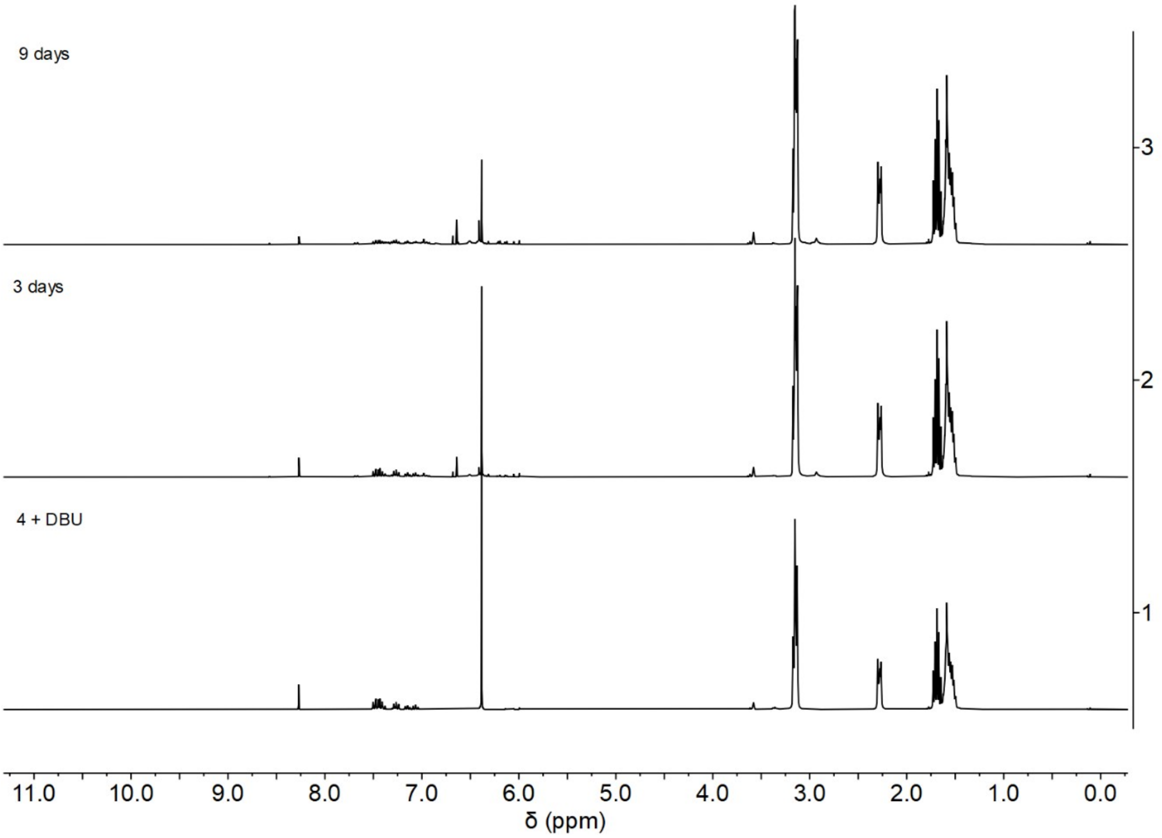

Figure S33. ^{1}H NMR spectrum (25 °C, 300 MHz, THF-d_8) of complex **4** after addition of DBU, after three and nine days (NMR tube was kept at room temperature).

5.5 Stability of complex 4 towards bases and hydrogen

The NMR tubes from the base stability experiments (complex **3** + base + CO_2, excluding the sample containing DBU) were frozen using liquid nitrogen and evacuated ($1\cdot10^{-3}$ mbar), followed by addition of hydrogen (1 bar pressure) to the evacuated tube. After thawing, NMR spectra were collected, then the tube was heated to 60°C and NMR spectra were collected at regular intervals. In the sample containing NEt_3, no visible change occurred, whereas in the sample containing pyridine, a solid began to precipitate and the colour changed, becoming darker and deep brown, then yellow/orange.

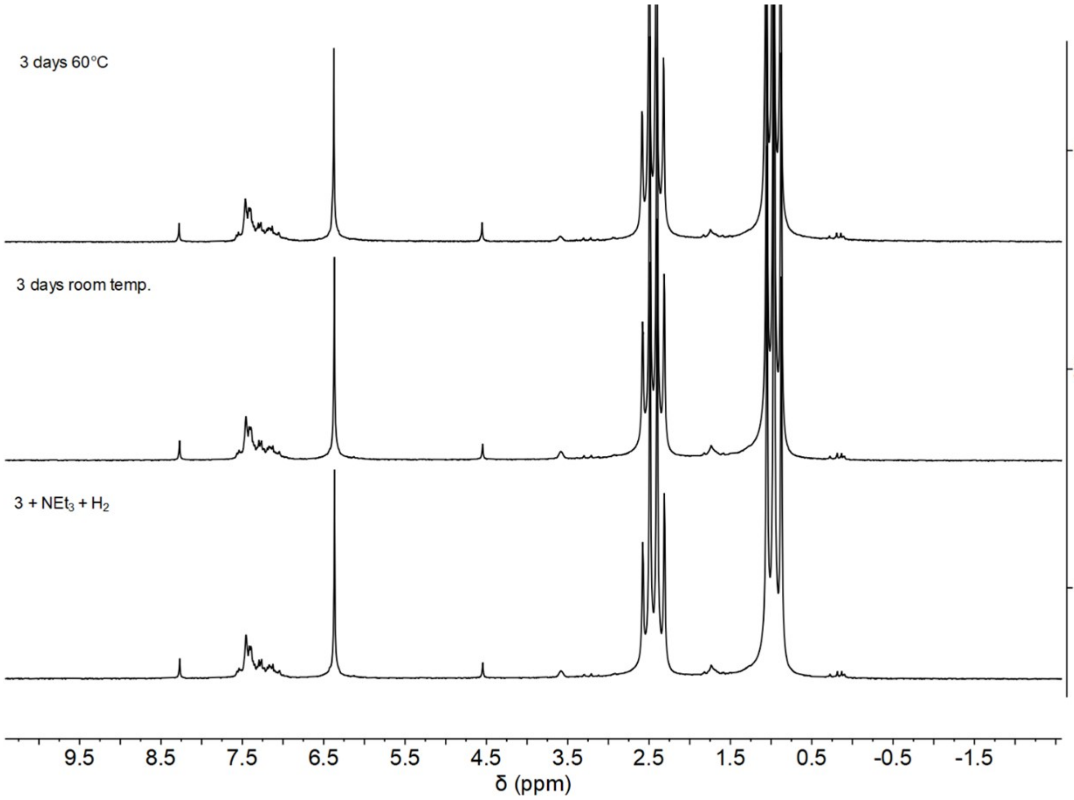

Figure S34. ^1H NMR spectrum (25 °C, 80 MHz, THF-d_8) of complex **3** and NEt_3 after addition of H_2, after keeping the NMR tube at room temperature for three days and after heating to 60 °C for three days.

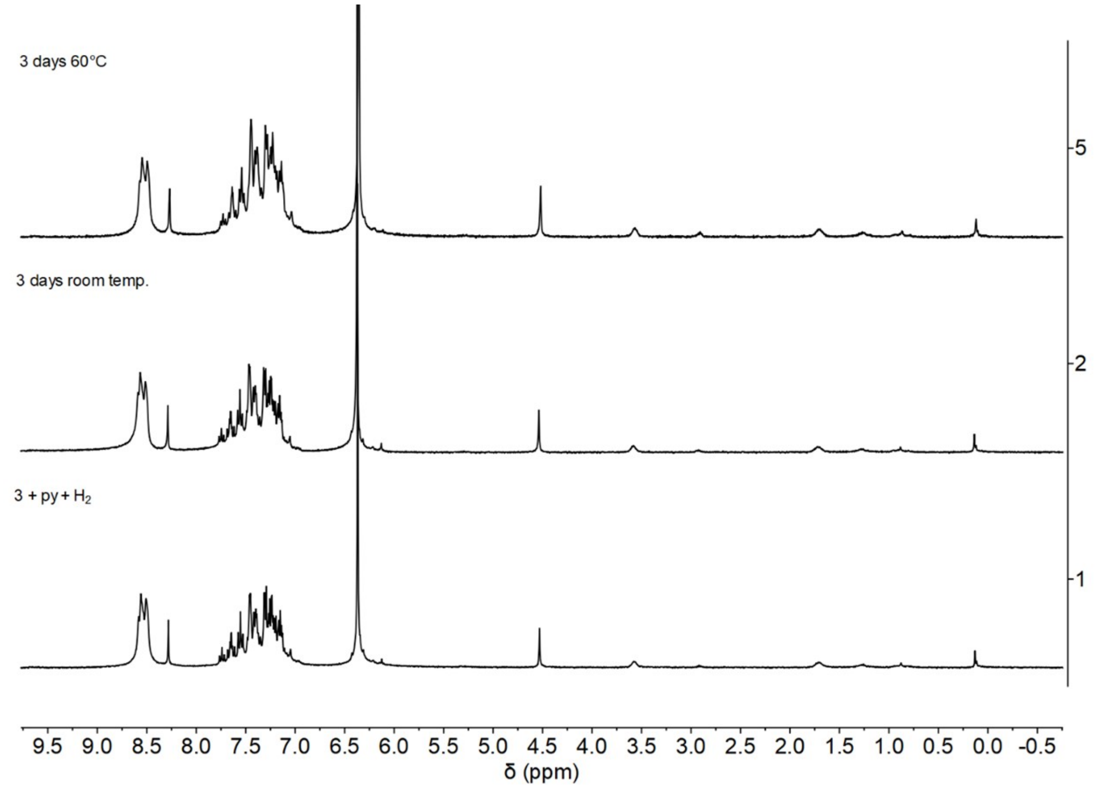

Figure S35. ^{1}H NMR spectrum (25 °C, 80 MHz, THF-d_8) of complex **3** and pyridine (py) after addition of H_2, after keeping the NMR tube at room temperature for three days and after heating to 60 °C for three days.

5.6 Reactivity of complex 4 with Et_2SiH_2

Complex **4** (17 mg, 0.037 mmol, 1 eq) was added to an NMR tube, dissolved in 0.6 mL of THF-d_8 and Et_2SiH_2 (5 µL, 0.037 mmol, 1 eq) was added using a Hamilton syringe. A ^1H NMR spectrum was recorded and then the NMR tube was heated to 50 °C for three hours.

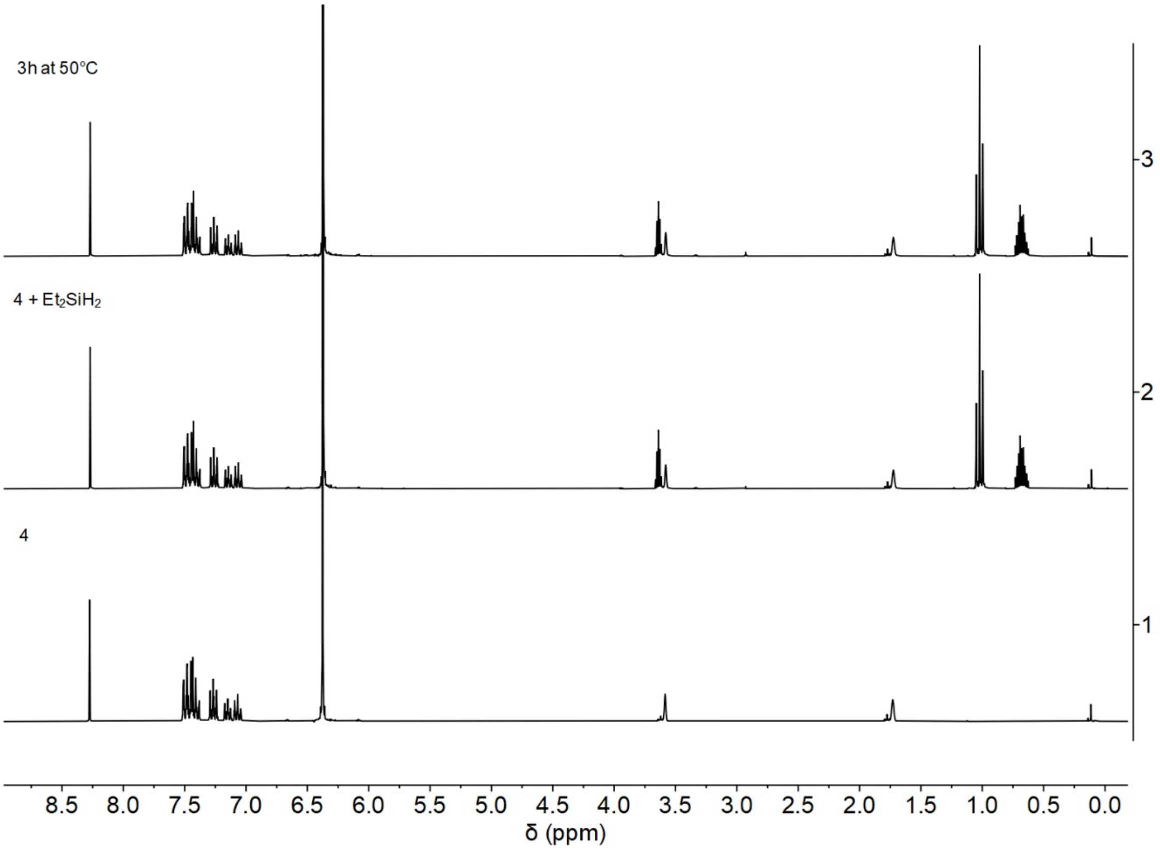

Figure S36. ^1H NMR spectrum (25 °C, 300 MHz, THF-d_8) of complex **4**, after addition of Et_2SiH_2 and after heating for 3 h to 50 °C.

6 Computational details

6.1 General Remarks

For a deeper understanding of the observed reaction behaviour, a two-step computational investigation was carried out. First, the observed reaction pathway and its possible transition states were investigated using the semi-empirical GFN2-xTB method,[12] followed by a DFT re-optimisation and verification at the B3LYP[13]-D3[14]/def2-TZVP[15] level (Notation: B3LYP-D3/def2-TZVP). Computations were carried out using *Gaussian16.*[16] The real-size molecules were optimised using the hybrid density functional method B3LYP. Vibrational frequencies were also computed, to include zero-point vibrational energies in thermodynamic parameters and to characterise all structures as minima on the potential energy surface. To confirm the accuracy of the calculated transition states (TS), intrinsic reaction coordinate (IRC) analysis was performed on these structures. Reaction profiles were compiled using EnePro v1.6.[17] In addition to the Supporting Information, we provide a multi-structure xyz file with all calculated molecules. For a better understanding and a more intuitive view of the calculated 3D structures, we strongly recommend using this file, e.g., with the free program MERCURY.[18]

Please note that all computations were carried out for single, isolated molecules in the gas phase (ideal gas approximation). There may well be significant differences between gas phase and condensed phase.

6.2 Quantum mechanical investigation of possible reaction pathways

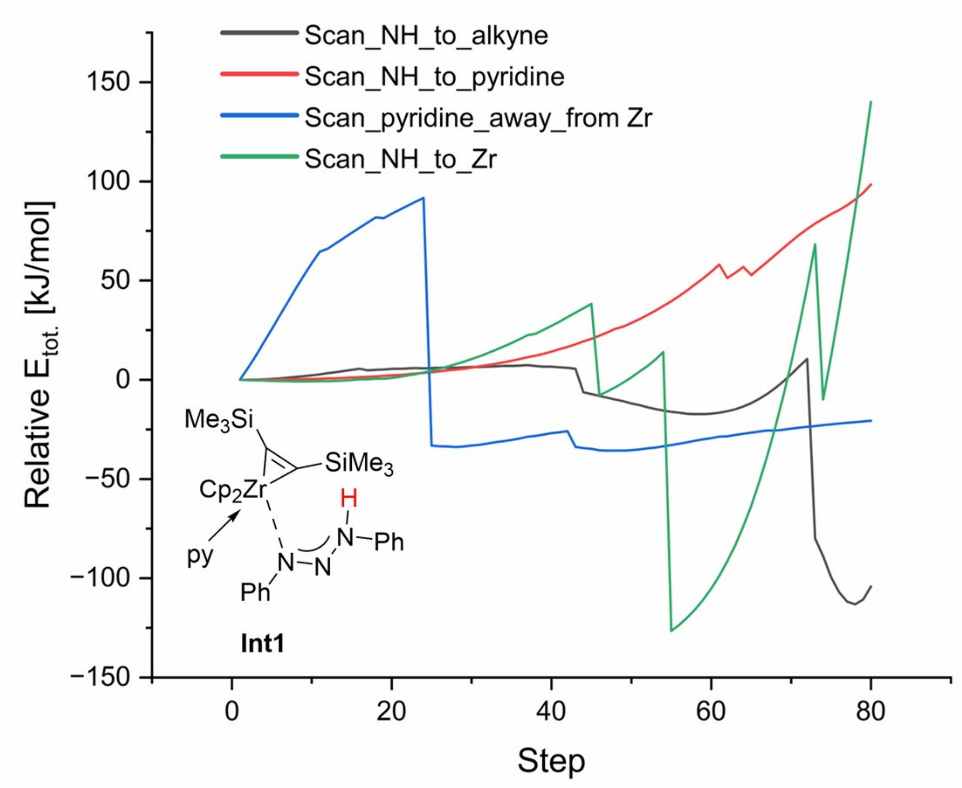

Figure S37. Four possible reaction pathways, starting from the **Int1** geometry, analysed in four different scans at the GFN2-xTB level of theory. The comparison of the relative energy profiles shows that the hydrogen shift to the pyridine as well as the pyridine de-coordination starting from this intermediate are rather unlikely. Interestingly, the hydrogen shift to the alkyne unit shows the lowest energy barrier and the second highest energy gain. This pathway is in line with the experimentally observed reaction. Therefore, this pathway was investigated further.

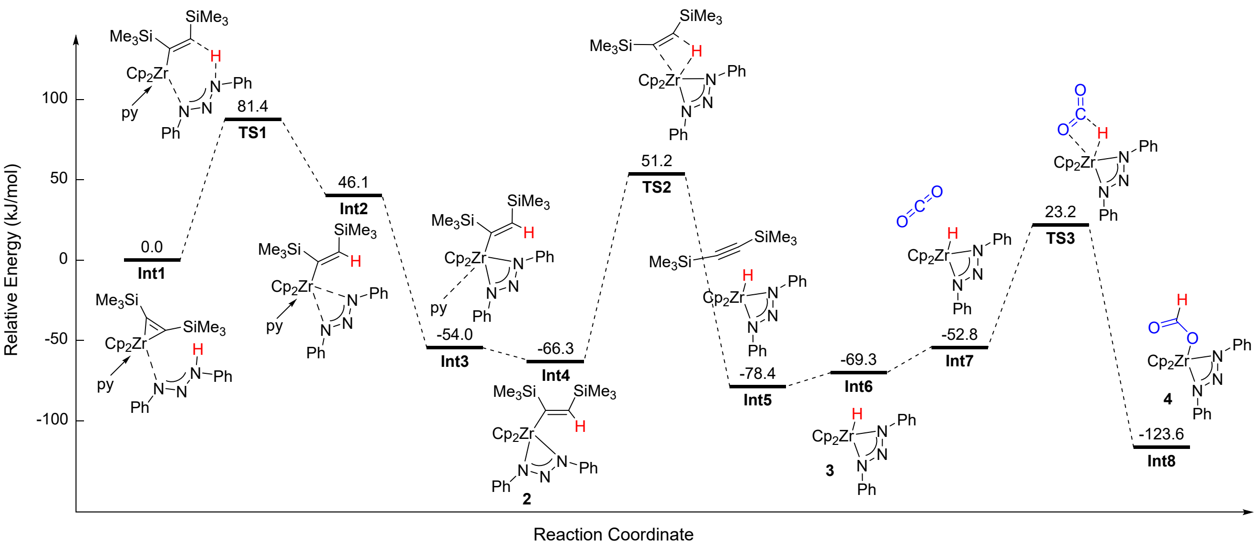

Figure S38. Calculated reaction profile in agreement with the observed reaction behaviour (B3LYP-D3/def2-TZVP, py = pyridine).

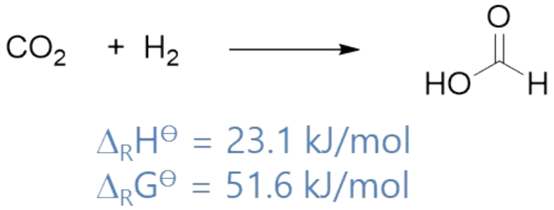

Figure S39. Calculated energies for formic acid formation (B3LYP-D3/def2-TZVP).

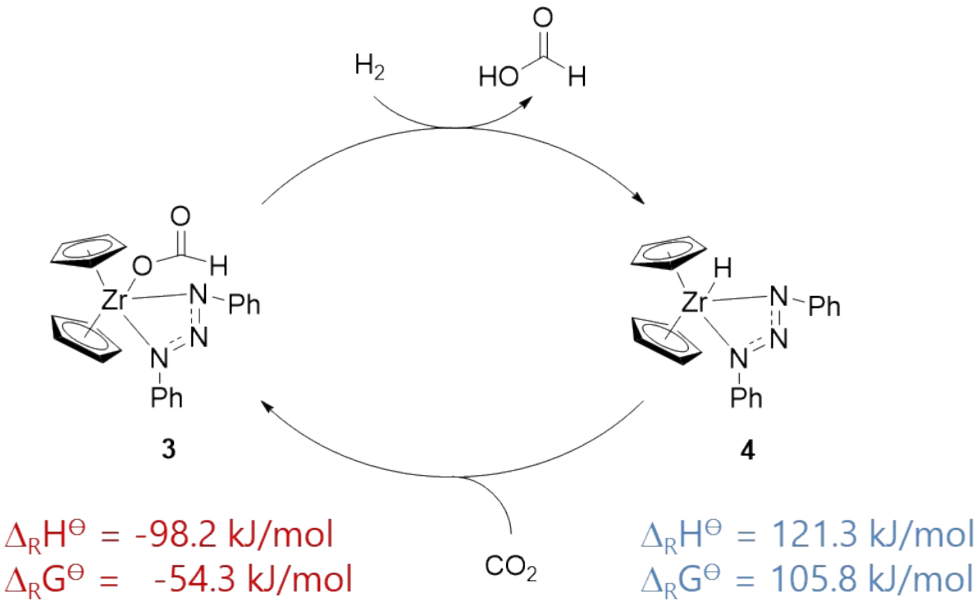

Figure S40. Calculated energies for a proposed catalytic profile for the formation of formic acid *via* complexes **3** and **4** (B3LYP-D3/def2-TZVP).

6.2.1 Total energies for all calculated compounds

Table S3. Summary of thermodynamic data of all calculated compounds level of theory B3LY-D3/def2-TZVP.

Compound	Nimag	E_{tot}	ZPE [kcal/mol]	H_{298} [a.u.]	G_{298} [a.u.]	Method	Basisset	calc
H2	0	-1.171094	6.209	-1.157894	-1.172741	B3LYP-D3	def2-SVPP	opt freq
CO2	0	-188.444680	7.390	-188.429325	-188.453606	B3LYP-D3	def2-SVPP	opt freq
HOCHO	0	-189.611489	21.158	-189.573680	-189.601844	B3LYP-D3	def2-SVPP	opt freq
Cp2ZrPhNNNPhH	0	-1061.691841	234.866	-1061.294111	-1061.371897	B3LYP-D3	def2-SVPP	opt freq
Cp2ZrPhNNNPhCHOO	0	-1250.184428	245.657	-1249.766098	-1249.850883	B3LYP-D3	def2-SVPP	opt freq
H2	0	-1.179790	6.315	-1.166421	-1.181216	B3LYP-D3	def2-TZVP	opt freq
CO2	0	-188.671581	7.345	-188.656318	-188.680564	B3LYP-D3	def2-TZVP	opt freq
HOCHO	0	-189.851719	21.116	-189.813956	-189.842143	B3LYP-D3	def2-TZVP	opt freq
pyridine	0	-248.396173	55.624	-248.302321	-248.334917	B3LYP-D3	def2-TZVP	opt freq
Me3SiCCSiMe3	0	-894.958400	145.977	-894.709804	-894.765801	B3LYP-D3	def2-TZVP	opt freq
PhNNNHPh iso1	0	-628.392357	129.942	-628.172224	-628.226232	B3LYP-D3	def2-TZVP	opt freq
PhNNNHPh TS	1	-628.360373	129.243	-628.141865	-628.194660	B3LYP-D3	def2-TZVP	opt freq
PhNNNHPh iso2	0	-628.386248	130.272	-628.165616	-628.221122	B3LYP-D3	def2-TZVP	opt freq
Cp2ZrpyPhNNNHPhMe3SiCCSiMe3 (**Int1**)	0	-2206.234210	440.701	-2205.483966	-2205.613579	B3LYP-D3	def2-TZVP	opt freq
Cp2ZrpyPhNNNHPhMe3SiCCSiMe3 (**TS1**)	1	-2206.199842	437.110	-2205.456218	-2205.582596	B3LYP-D3	def2-TZVP	opt freq
Cp2ZrpyPhNNNPhMe3SiCCHSiMe3 (**Int2**)	0	-2206.217363	440.024	-2205.468819	-2205.596011	B3LYP-D3	def2-TZVP	opt freq
Cp2ZrPhNNNPhMe3SiCCHSiMe3 py (**Int3)**	0	-2206.253896	440.550	-2205.504106	-2205.634136	B3LYP-D3	def2-TZVP	opt freq
Cp2ZrPhNNNPhMe3SiCCHSiMe3 iso1 (**Int4**)	0	-1957.844150	383.963	-1957.190854	-1957.303922	B3LYP-D3	def2-TZVP	opt freq
Cp2ZrPhNNNPhMe3SiCCHSiMe3 TS H shift iso1 (**TS2**)	1	-1957.789259	379.802	-1957.141829	-1957.259148	B3LYP-D3	def2-TZVP	opt freq
Cp2ZrHPhNNNPhMe3SiCCSiMe3 (**Int5**)	0	-1957.837510	380.775	-1957.187863	-1957.308529	B3LYP-D3	def2-TZVP	opt freq
Cp2ZrHPhNNNPh **3** (**Int6**)	0	-1062.857213	233.940	-1062.460760	-1062.539272	B3LYP-D3	def2-TZVP	opt freq
Cp2ZrHCO2PhNNNPh (**Int7**)	0	-1251.536047	241.808	-1251.122705	-1251.213529	B3LYP-D3	def2-TZVP	opt freq
Cp2ZrHCO2PhNNNPh (**TS3**)	1	-1251.515275	243.242	-1251.101251	-1251.184587	B3LYP-D3	def2-TZVP	opt freq
Cp2ZrPhNNNPhCHO2 (**Int8**)	0	-1251.571433	244.644	-1251.154480	-1251.240508	B3LYP-D3	def2-TZVP	opt freq
Cp2ZrMe3SiCCSiMe3py **1** (**Int1_2**)	0	-1577.820712	308.687	-1577.294058	-1577.393913	B3LYP-D3	def2-TZVP	opt freq
Cp2ZrPhNNNHPhMe3SiCCSiMe3 iso1 **2** (**Int2_2**)	0	-1957.807600	382.777	-1957.154927	-1957.274018	B3LYP-D3	def2-TZVP	opt freq
Cp2ZrPhNNNHPhMe3SiCCSiMe3 iso3 **2** (**Int2_3**)	0	-1957.798157	382.754	-1957.145610	-1957.262605	B3LYP-D3	def2-TZVP	opt freq
Cp2ZrPhNNNHPhMe3SiCCSiMe3 iso2 **2** (**Int2_4**)	0	-1957.800191	382.811	-1957.147608	-1957.265924	B3LYP-D3	def2-TZVP	opt freq
Cp2ZrPhNNNHPhMe3SiCCSiMe3 cleav. (**Int3_2**)	0	-1957.802737	382.351	-1957.150362	-1957.271049	B3LYP-D3	def2-TZVP	opt freq
Cp2ZrPhNNNPhMe3SiCCHSiMe3 iso2 (**Int3_3**)	0	-1957.840986	384.423	-1957.187217	-1957.187217	B3LYP-D3	def2-TZVP	opt freq
Cp2ZrPhNNNHPh iso1 (**Int4_2**)	0	-1062.820320	235.146	-1062.421771	-1062.499006	B3LYP-D3	def2-TZVP	opt freq
Cp2ZrPhNNNHPh iso2 (**Int5_2**)	0	-1062.829769	235.857	-1062.430274	-1062.507511	B3LYP-D3	def2-TZVP	opt freq
Cp2ZrPhNNNHPh (**TS1_2**)	1	-1062.790538	232.427	-1062.396793	-1062.474179	B3LYP-D3	def2-TZVP	opt freq
Cp2ZrPhNNNPhMe3SiCCHSiMe3 TS H shift iso2 (**TS2_2**)	1	-1957.785822	380.352	-1957.137504	-1957.254718	B3LYP-D3	def2-TZVP	opt freq
Cp2ZrPhNNNHPhMe3SiCCSiMe3 **TS** H shift (**TS1**)	1	-1957.743098	379.032760	-1957.097193	-1957.213161	B3LYP-D3	def2-TZVP	opt freq

7 References

1 J. R. Nitschke, S. Zürcher and T. D. Tilley, *J. Am. Chem. Soc.*, 2000, **122**, 10345-10352.

2 W. W. Hartman and J. B. Dickey, *Organic Syntheses*, 1934, **14**, 24.

3 G. R. Fulmer, A. J. Miller, N. H. Sherden, H. E. Gottlieb, A. Nudelman, B. M. Stoltz, J. E. Bercaw, and K. I. Goldberg, *Organometallics*, 2010, **29**, 2176-2179.

4 a) D. H. Live, D. G. Davis, W. C. Agosta and D. Cowburn, *J. Am. Chem. Soc.*, 1984, **106**, 1939-1941; b) R. K. Harris, E. D. Becker, S. M. Cabral de Menezes, R. Goodfellow and P. Granger, *Pure Appl. Chem.*, 2001, **73**, 1975-1818; c) R. K. Harris, E. D. Becker, S. M. Cabral de Menezes, P. Granger, R. E. Hoffman and K. W. Zilm, *Pure Appl. Chem.*, 2008, **80**, 59-84.

5 S. Chen, J. Wang and H. Wang, *Materials & Design*, 2016, **90**, 84-90.

6 G. M. Sheldrick, *Acta Cryst., Sect. A: Found. Crystallogr.*, 2008, **64**, 112-122.

7 G. M. Sheldrick, *Acta Cryst., Sect. C: Struct. Chem.*, 2015, **71**, 3-8.

8 Diamond - Crystal and Molecular Structure Visualization, Crystal Impact - Dr. H. Putz & Dr. K. Brandenburg GbR, Kreuzherrenstr. 102, 53227 Bonn, Germany, http://www.crystalimpact.com/diamond.

9 S. Berger, S. Braun and H.-O. Kalinowski, *NMR-Spektroskopie von Nichtmetallen, Vol. 2: ^{15}N-NMR-Spektroskopie.* G. Thieme Verlag, Stuttgart, **1992**. In particular Section 2.7.3 and refs. given therein.

10 E. Lippmaa, T. Saluvere, T. Pehk and A. Olivson, *Organic Magnetic Resonance*, 1973, **5**, 429-436. Note that chemical shifts in this work are given with respect to the nitrate anion. 4 ppm has been subtracted from these values to convert them to the nitromethane scale.

11 G. Albertin, S. Antoniutti, M. Bedin, J. Castro and S. García-Fontán, *Inorg. Chem.*, 2006, **45**, 3816-3825.

12 C. Bannwarth, S. Ehlert and S. Grimme, *J. Chem. Theory Comput.*, 2019, **15**, 1652–1671.

13 A. D. Becke, *J. Chem. Phys.*, 1993, **98**, 5648-5652.

14 S. Grimme, S. Ehrlich and L. Goerigk, *J. Comput. Chem.*, 2011, **32**, 1456-1465.

15 F. Weigend and R. Ahlrichs, *Phys. Chem. Chem. Phys.*, 2005, **7**, 3297-3305.

16 Gaussian 16, Revision C.01, M. J. Frisch, G. W. Trucks, H. B. Schlegel, G. E. Scuseria, M. A. Robb, J. R. Cheeseman, G. Scalmani, V. Barone, G. A. Petersson, H. Nakatsuji, X. Li, M. Caricato, A. V. Marenich, J. Bloino, B. G. Janesko, R. Gomperts, B. Mennucci, H. P. Hratchian, J. V. Ortiz, A. F. Izmaylov, J. L. Sonnenberg, D. Williams-Young, F. Ding, F. Lipparini, F. Egidi, J. Goings, B. Peng, A. Petrone, T. Henderson, D. Ranasinghe, V. G. Zakrzewski, J. Gao, N. Rega, G. Zheng, W. Liang, M. Hada, M. Ehara, K. Toyota, R. Fukuda, J. Hasegawa, M. Ishida, T. Nakajima, Y. Honda, O. Kitao, H. Nakai, T. Vreven, K. Throssell, J. A. Montgomery, Jr., J. E. Peralta, F. Ogliaro, M. J. Bearpark, J. J. Heyd, E. N. Brothers, K. N. Kudin, V. N. Staroverov, T. A. Keith, R. Kobayashi, J. Normand, K. Raghavachari, A. P. Rendell, J. C. Burant, S. S. Iyengar, J. Tomasi, M. Cossi, J. M. Millam, M. Klene, C. Adamo, R. Cammi, J. W. Ochterski, R. L. Martin, K. Morokuma, O. Farkas, J. B. Foresman, and D. J. Fox, Gaussian, Inc., Wallingford CT, 2016.

17 Z. Wang, EnePro version1.6 2021.

18 Mercury: http://www.ccdc.cam.ac.uk/mercury/